

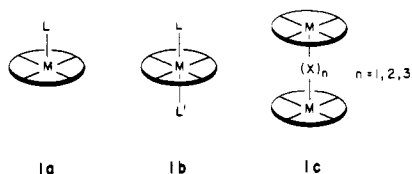
## Metalloporphyrins with Unusual Geometries. 2. Slipped and Skewed Bimetallic Structures, Carbene and Oxo Complexes, and Insertions into Metal-Porphyrin Bonds

KAZUYUKI TATSUMI and ROALD HOFFMANN\*

Received May 15, 1981

The electronic factors determining the unusual geometries of slipped and skewed out-of-plane metalloporphyrins, carbene-complexed porphyrins, and acetylene adducts of macrocycles are the subject of this study. Orbital diagrams constructed for  $[\text{Re}(\text{CO})_3]_2\text{N}_4$  and  $[\text{Rh}(\text{CO})_2]_2\text{N}_4$ , where  $\text{N}_4$  is a model porphyrin, explain why the  $\text{Re}(\text{CO})_3$  and  $\text{Rh}(\text{CO})_2$  fragments tend to slip off the  $S_2$  axis normal to the porphyrin plane. We predict a large rotational barrier for each fragment in its slipped-off geometries. A carbene fragment in a metalloporphyrin should insert into an M-N bond when the molecule has a  $d^8$  electronic configuration and/or the d orbitals of the central metal are lowered in energy. Through an analogy between the electronic structure of  $d^4$  oxo complexes  $\text{Fe}(\text{porphyrin})(\text{O})$ , and that of  $d^8$  carbene complexes  $\text{Ni}(\text{porphyrin})(\text{CR}_2)$ , it is suggested that an intramolecular oxygen migration in  $d^4$  oxo porphyrin complexes is a possible reaction channel. The calculated energy surface for the acetylene adduct of  $\text{Co}^{\text{III}}(\text{TAA})(\text{NH}_2)$  reproduces the observed trend that acetylene is added across the six-membered chelate ring of  $\text{Co}^{\text{III}}(\text{TMTAA})(\text{py})^+$ . However, the addition of acetylene to a  $d^6$  central metal is also a possibility, if the metal has diffuse high-energy d orbitals.

Most metalloporphyrins are rather simply described, from a structural viewpoint. A porphyrin complex usually consists of a porphyrin ring, mildly distorted from planarity, and a metal ion, the latter sitting squarely in the middle of the porphyrin ring. Occasionally a metal atom takes up one or two ligands to complete a square-pyramidal, **1a**, or octahedral,

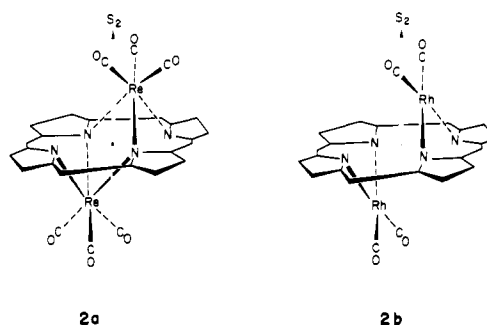


**1b**, coordination sphere. Variety and versatility are provided by displacement of the metal atom out of the coordination plane and the ability of almost every element in the periodic table to enter the macrocycle. The mono-, di-, and tri-bridged porphyrin dimers, **1c**, which formed the subject of part 1 of our study,<sup>1</sup> still retain at each metal atom the basic metalloporphyrin type.

Some recently synthesized porphyrins, however, are not reconciled to a limitation of their geometrical freedom to the normal monometallic porphyrin paradigm. They slip, twist, and skew in remarkable ways. Recognition of geometrical variety was one motive for the initiation of our theoretical study of metalloporphyrins. In this second part, we look at skewed out-of-plane metalloporphyrins ( $\text{ML}_n$ )<sub>2</sub>(porphyrin) (M = Tc, Re, Rh), carbene-complexed porphyrins and, related to them, metalloporphyrins in which a carbene inserts into a M-N bond, and acetylene adducts of a macrocycle related to the porphyrins. In all of these complexes, the ring departs from its role as a simple quadruplet of nitrogen donors. We will also analyze the electronic structure of some oxo-iron porphyrin complexes formally analogous to carbene-metalloporphyrin complexes.

**Slipped Geometry of  $[\text{M}(\text{CO})_n]_2$ (porphyrin) Complexes.** The reaction of  $\text{Re}_2(\text{CO})_{10}$  with porphyrin yields several different rhenium porphyrin complexes, depending on the porphyrin ring and the ratio of the reactants.<sup>2</sup> Among the compounds isolated, one is well characterized in which two  $\text{Re}(\text{CO})_3$  fragments sandwich a porphyrin ring:  $[\text{Re}(\text{CO})_3]_2\text{TPP}$  (TPP =

mesotetraphenylporphyrin). In this unusual structure, each  $\text{Re}(\text{CO})_3$  moves off the  $S_2$  axis normal to the porphyrin plane, as shown in **2a**.  $[\text{Tc}(\text{CO})_3]_2\text{TPP}$ , which isoelectronic to



$[\text{Re}(\text{CO})_3]_2\text{TPP}$ ,<sup>1a</sup> and a related compound  $[\text{Re}(\text{CO})_3]_2\text{TAA}$  (TAA = dibenzo[*b,i*]-1,4,8,11-tetraaza[14]annulene)<sup>2b</sup> have structures very similar to **2a**. Likewise each  $\text{Rh}(\text{CO})_2$  fragment in  $[\text{Rh}(\text{CO})_2]_2\text{OEP}$ <sup>3</sup> (OEP =  $\mu$ -(1,2,3,4,5,6,7,8-octaethylporphyrin)), is slipped off the  $S_2$  axis, **2b**.

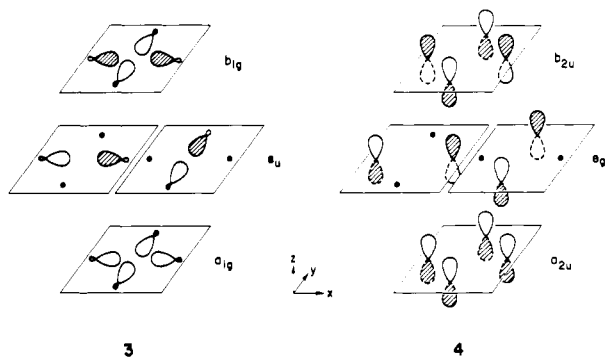
Why are these fragments not positioned directly over the center of the ring? Our theoretical analysis of the unusual skewed geometries begins by constructing the valence orbitals of  $[\text{Re}(\text{CO})_3]_2\text{N}_4$ . The " $\text{N}_4$ " unit is a model for a porphyrin,  $(\text{NH}_2)_4^{4-}$ . It is the smallest and reasonably reliable model which we have found in a progressive simplification of the porphyrin ring.<sup>1</sup> Our construction requires knowledge of the energy levels of " $\text{N}_4$ " =  $(\text{NH}_2)_4^{4-}$  and  $\text{Re}(\text{CO})_3^+$  building blocks.

The orbitals of  $D_{4h}$   $(\text{NH}_2)_4$  are made up of combinations of N lone pairs and N  $p_\pi$ 's. The four N lone pairs which point at the center of the  $(\text{NH}_2)_4$  plane provide one set of molecular orbitals,  $b_{1g}$ ,  $e_u$ , and  $a_{1g}$ , as shown in **3**. The combinations of four N  $p_\pi$  orbitals are  $b_{2u}$ ,  $e_g$ , and  $a_{2u}$  as in **4**. These eight levels are all doubly occupied in the  $(\text{NH}_2)_4^{4-}$  electron count which corresponds to a dianionic porphyrin ring.

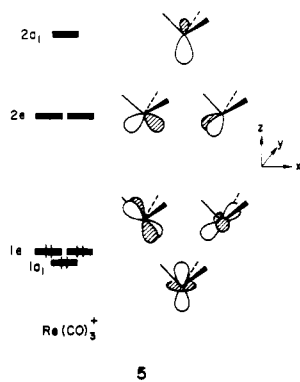
(1) Part 1: Tatsumi, K.; Hoffmann, R. *J. Am. Chem. Soc.* **1981**, *103*, 3328-3341.

(2) (a) Ostfeld, D.; Tsutsui, M.; Hrung, C. P.; Conway, D. C. *J. Am. Chem. Soc.* **1971**, *93*, 2548-2549. Cullen, D.; Meyer, Jr., E. F.; Srivastava, S.; Tsutsui, M. *Ibid.* **1972**, 7603-7605. Tsutsui, M.; Hrung, C. P. *Ibid.* **1973**, *95*, 5777-5778. Tsutsui, M.; Hrung, C. P.; Ostfeld, D.; Srivastava, T. S.; Cullen, D. L.; Meyer, Jr., E. F. *Ibid.* **1975**, *97*, 3952-3965. (b) Tsutsui, M.; Bobsein, R. L.; Pettersen, R.; Haaker, R. *J. Coord. Chem.* **1979**, *8*, 245-248.

(3) Takenaka, A.; Sasada, Y.; Omura, T.; Ogoshi, H.; Yoshida, Z. *J. Chem. Soc., Chem. Commun.* **1973**, 792-793; *Acta Crystallogr., Sect. B* **1975**, *B31*, 1-6.



The molecular orbitals of an  $ML_3$  fragment in  $C_{3v}$  geometry have been described in the literature.<sup>4a-c,5</sup> We give only the basic energy ordering and a brief sketch of the frontier orbitals of  $Re(CO)_3^+$  in 5. There is a nest of three low-lying orbitals,



$a_1 + e$ , composed mainly of  $Re\ z^2$  ( $1a_1$ ),  $xy$ , and  $x^2 - y^2$  ( $1e$ ). At somewhat higher energy is another  $e$  set, primarily of  $xz$ ,  $yz$  character ( $2e$ ). The mixing between  $xy$  and  $xz$ , or between  $x^2 - y^2$  and  $yz$ , in each  $e$  set results in a tilting of the four  $d$  orbitals from their axes. At still higher energy, there is an  $a_1$  level, composed of  $Re\ s$ ,  $p$ , and a substantial contribution of  $z^2$  ( $2a_1$ ).

The orbitals of  $[Re(CO)_3]_2N_4$  are built up in Figure 1. Throughout this paper we use extended Hückel calculations, with parameters given in the Appendix. The  $Re$  atoms sit above and below the center of the " $N_4$ ", i.e., on the  $S_2$  axis. On the right side of the figure, the two  $Re(CO)_3^+$  fragments are brought to 3.12-Å separation in a staggered  $D_{3d}$  geometry. In the absence of the central  $(NH_2)_4^{4+}$  unit, the direct through-space interaction of the  $Re(CO)_3^+$  orbitals is small, except for the diffuse  $2a_1$  orbital which is not shown in the figure. The  $d$ -block levels are then simply in- and out-of-phase pairs of each  $Re(CO)_3^+$  fragment orbital. At the left there are a set of occupied  $\pi$  and lone-pair orbitals of the  $(NH_2)_4^{4+}$  unit. These are all lower in energy than the  $(CO)_3Re \cdots Re(CO)_3$  framework orbitals. Thus the "insertion" of  $(NH_2)_4^{4+}$  destabilizes the  $d$  block. Of the six occupied  $d$  levels, the  $2a_g$  and  $2b_u$  are most strongly destabilized by an anti-

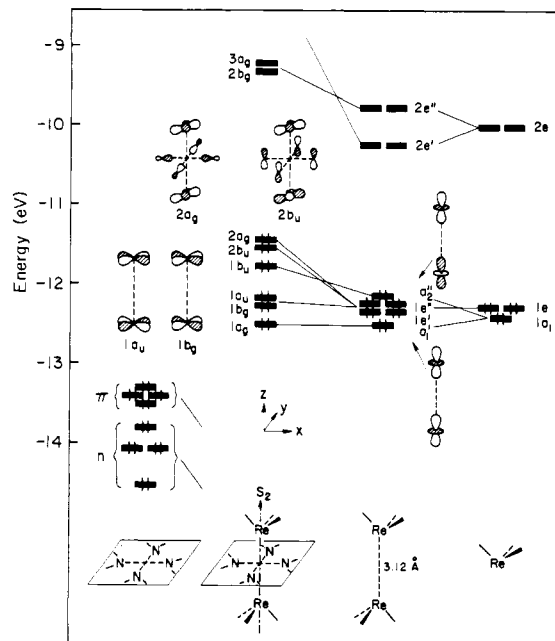


**Figure 1.** Interaction diagram for the valence orbitals of  $[Re(CO)_3]_2N_4$ . At right, two  $Re(CO)_3^+$  fragments are combined, held in a  $D_{3d}$  geometry. Then the  $[Re(CO)_3]_2^{2+}$  composite is mixed with  $(NH_2)_4^{4+}$  at left.

bonding interaction with  $b_{1g}$  ( $n^*$ ) and  $b_{2u}$  ( $\pi^*$ ) of the  $D_{4h}$   $(NH_2)_4^{4+}$ .

Please note the electron count in Figure 1. It is for  $Re_2(CO)_6(NH_2)_4^{2-}$ , which in turn serves as a model for  $Re_2(CO)_6(TPP)$ . The electronic configuration is  $d^6$  at each metal, so that the entire lower  $d$  block is occupied.

The structure of  $[Re(CO)_3]_2(TPP)^+$  supports the calculated antibonding character of the highest occupied level,  $2a_g$  or  $2b_u$ .<sup>6</sup> When one electron is removed from  $[Re(CO)_3]_2(TPP)$ , the  $Re-N$  and  $Re-Re$  distances are all shortened. The three short  $Re-N$  distances 2.17, 2.38, and 2.41 Å in  $[Re(CO)_3]_2(TPP)$  are reduced to 2.11, 2.35, and 2.36 Å in the monocation. The  $Re-Re$  distance also becomes shorter by 0.18 Å.

Even at this point we can comment on the likelihood of deformation. The two highest occupied orbitals bear substantial  $Re-N_4$  antibonding character. This destabilizing feature would be eased if the  $Re(CO)_3$  units were to slip off the  $S_2$  axis.

Before analyzing the deformation, let us look at the orbital structure of the complex in more detail. At the positions 1.56 Å above and below the center of the  $(NH_2)_4$  plane, the  $Re\ xy$ ,  $x^2 - y^2$ ,  $xz$ , and  $yz$  orbitals in  $1b_g$ ,  $1a_u$ ,  $2b_u$ ,  $2a_g$ , and the upper unoccupied  $2b_g$  and  $3a_g$  levels still tilt off their axes, just as would the orbitals of an isolated  $Re(CO)_3$  unit. This tilting was found to be important in determining rotational barriers in polyene- $ML_3$  transition-metal complexes.<sup>5</sup> In the case of the unslipped  $[Re(CO)_3]_2N_4$ , the calculated barrier for a simultaneous rotation of two rigid  $Re(CO)_3$  groups against the fixed framework is essentially zero. No wonder, for the barrier is 12-fold. The barrier will not remain so small when the  $Re(CO)_3$  groups are allowed to slip off the axis.

Now consider a slipping sideways of the  $Re(CO)_3$  groups, one in the  $+x$  direction, the other in the  $-x$  direction, starting in the geometry illustrated in Figure 1 and reproduced in projection 6 below. With the  $Re$  atom kept 1.56 Å above the  $N_4$  plane and with the  $Re$  atom confined to a plane containing two nitrogens, there remain two nonequivalent deformations,

(4) (a) Orgel, L. E. *J. Inorg. Nucl. Chem.* **1956**, *2*, 315-322. (b) Kettle, S. F. A. *Inorg. Chem.* **1965**, *4*, 1661-1663. (c) Whitesides, T. H.; Lichtenberger, D. L.; Budnik, R. A. *Ibid.* **1975**, *14*, 68-73. Lichtenberger, D. L.; Fenske, R. F. *J. Am. Chem. Soc.* **1976**, *98*, 50-63. (d) Burdett, J. K. *Inorg. Chem.* **1975**, *14*, 375-382; *J. Chem. Soc., Faraday Trans. 2* **1974**, *70*, 1599-1613. (e) Elian, M.; Hoffmann, R. *Inorg. Chem.* **1975**, *14*, 1058-1076. Elian, M.; Chen, M. M. L.; Mingos, D. M. P.; Hoffmann, R. *Ibid.* **1976**, *15*, 1148-1155. Summerville, R. H.; Hoffmann, R. *J. Am. Chem. Soc.* **1979**, *101*, 3821-3831. Schilling, B. E. R.; Hoffmann, R. *Ibid.* **1979**, *101*, 3456-3467. (f) Mingos, D. M. P. *J. Chem. Soc., Dalton Trans.* **1977**, 602-610. (g) Hoffmann, P. *Angew. Chem.* **1977**, *89*, 551-553. (h) Albright, T. A.; Hoffmann, R.; Thibeault, J. C.; Thorn, D. L. *J. Am. Chem. Soc.* **1979**, *101*, 3801-3812. Jemmis, E. D.; Hoffmann, R. *Ibid.* **1980**, *102*, 2570-2575. (5) Albright, T. A.; Hoffmann, P.; Hoffmann, R. *Ibid.* **1977**, *99*, 7546-7557.

(6) Kato, S.; Tsutsui, M.; Cullen, D. L.; Meyer, Jr., E. F. *Ibid.* **1977**, *99*, 620-622.

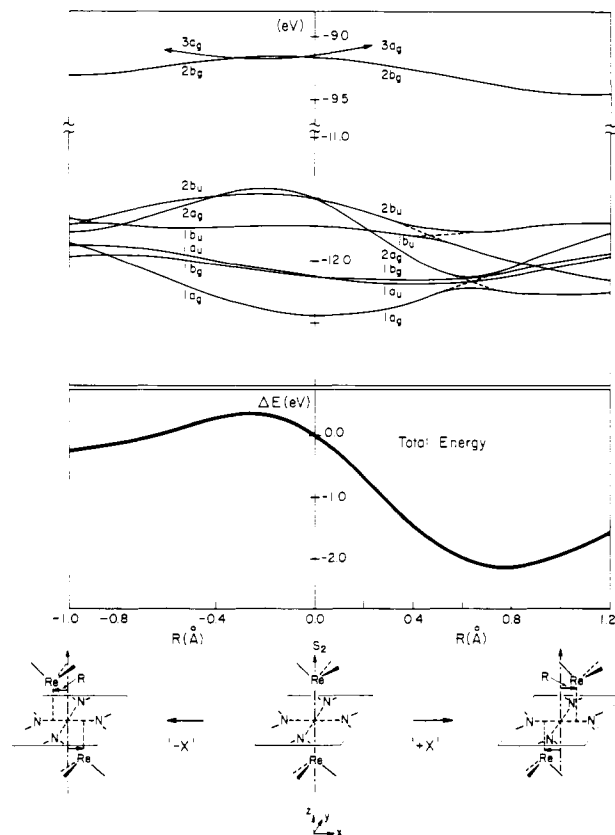


**Figure 2.** Walsh diagram (top) and the total energy curve (bottom) for the  $\text{Re}(\text{CO})_3$  groups slipping off the  $S_2$  axis in the '+X' and the '-X' directions. The two Re atoms are kept 1.56 Å above and below the  $N_4$  plane. The highest occupied molecular orbital is  $2b_u$  or  $2a_g$ , whichever comes at higher energy.

which we call '-X' (7) and '+X' (8).  $R$  measures the lateral slipping from point above or below the center of  $N_4$ .

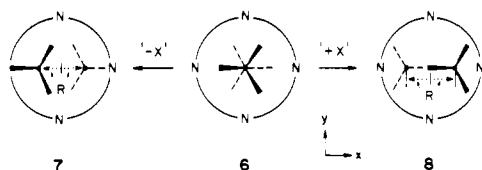
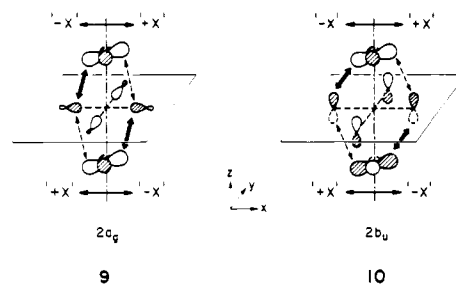


Figure 2 plots the change in the total energy as a function of  $R$ . Also shown are the energies of the valence orbitals. The HOMO is either the  $2a_g$  or  $2b_u$ , and the LUMO is the  $2b_g$ . The right side of the figure shows the energies for the '+X' deformation while the left side is for '-X'. The energetics clearly show that the unslipped geometry is not stable. Slipping in the '+X' manner stabilizes the molecule substantially. The energy minimum comes at  $R = 0.75$  Å, whereas the experimental value of  $R$  is 0.7–0.8 Å. The quantitative agreement may be fortuitous but supports the qualitative analysis. The Walsh diagram of Figure 2 shows that the major factor in the stabilization is indeed the behavior of the highest occupied  $2a_g$  and  $2b_u$  levels.

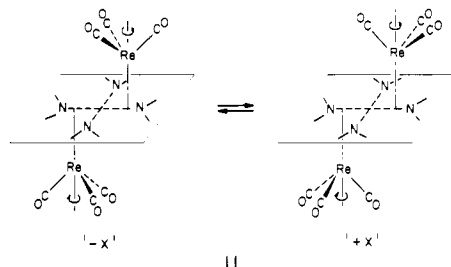
Deformation '-X' differs markedly from '+X'. At small  $R$ , the '-X' total energy curve actually goes up. Even at large  $R$  the stabilization along '-X' is not nearly as great as '+X'. For instance, at  $R = 0.8$  Å, '-X' is stabilized by -2.06 eV, '-X' by only -0.06 eV. The experimentally observed structure slips in the '+X' mode, in accord with the calculated surface. The contrasting behavior may be traced to the  $2b_u$  and  $2a_g$  levels. Upon '-X' deformation the two levels are first destabilized, while the '+X' deformation stabilizes them. The difference is a consequence of the tilting of Re  $x^2 - y^2$  orbitals, as

schematically shown in 9 and 10. The net antibonding in-



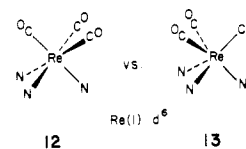
teractions of the tilted  $x^2 - y^2$  with the " $N_4$ " orbitals are first increased at small  $R$  of the '-X' mode.

The '+X' and '-X' conformations are, of course, interchanged at any  $R$  by simultaneous rotation of both  $\text{Re}(\text{CO})_3$  groups by 60 or 180°, as indicated in 11. The computed



potential curve of Figure 2 indicates that the barrier to this process is large, more than 2 eV at  $R = 0.8$  Å. Contrast that computed value with the near-zero barrier (0.001 kcal/mol) at  $R = 0$  Å.

The large barrier to  $\text{Re}(\text{CO})_3$  rotation which we calculate can be related to the stereochemical rigidity of the octahedral geometry of six-coordinate  $d^6$  transition-metal complexes. In the slipped  $[\text{Re}(\text{CO})_3]_2N_4$ , each Re metal sets up a coordination sphere such that three carbon and three adjacent nitrogen atoms occupy six coordination sites. The '+X' deformation forms an approximate octahedron at each Re, 12, while



'-X' leads to a trigonal prismatic environment, 13. The molecular orbital analysis of the trigonal twist between the octahedron and the trigonal prism is well established.<sup>7</sup> The preference for the octahedron, i.e., the rigidity of the octahedral geometry, is maximal for low-spin  $d^6$  complexes.

We turn to the skewed geometry of  $[\text{Rh}(\text{CO})_2]_2\text{OEP}$ . The analysis will follow a line similar to the one which we have employed for  $[\text{Re}(\text{CO})_3]_2\text{TPP}$ . Figure 3 constructs the molecular orbitals of a nonskewed model metalloporphyrin  $[\text{Rh}(\text{CO})_2]_2N_4$  with  $D_{2h}$  symmetry. The left side of the figure shows the  $\pi$  and lone pair orbital sets of the  $N_4$ . Note that the  $N_4$  unit is rotated by 45° in the  $xy$  plane from the position defined in Figure 1. Thus the  $x$  and  $y$  axes now lie in between two adjacent nitrogen atoms. At the right, a  $\text{Rh}(\text{CO})_2$  fragment carries six valence orbitals.<sup>4f-b</sup> The four lower levels are primarily made up of Rh  $d$  orbitals, assigned to  $1a_1$  ( $z^2$ ),  $1b_1$

(7) (a) Tomlinson, A. A. *G. J. Chem. Soc. A* **1971**, 1409–1414. (b) Gillum, W. O.; Wentworth, R. A. D.; Childers, R. F. *Inorg. Chem.* **1970**, *9*, 1825–1832. Wentworth, R. A. D. *Coord. Chem. Rev.* **1972**, *9*, 171–187. (c) Huisman, R.; De Jonge, R.; Haas, C.; Jellinek, F. J. *Solid State Chem.* **1971**, *3*, 56–66. (d) Larsen, E.; LaMar, G. N.; Wagner, B. F.; Parks, J. E.; Holm, R. H. *Inorg. Chem.* **1972**, *11*, 2652–2668. (e) Hoffmann, R.; Howell, J. M.; Rossi, A. R. *J. Am. Chem. Soc.* **1976**, *98*, 2484–2492.

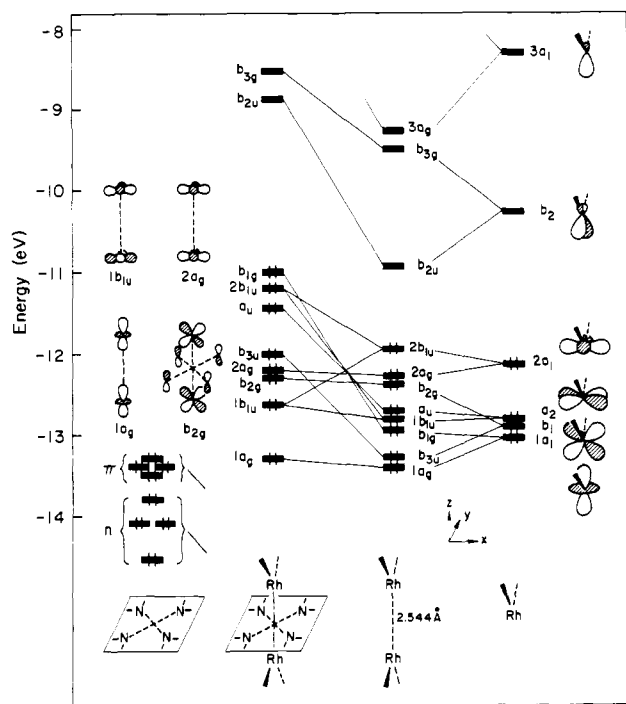
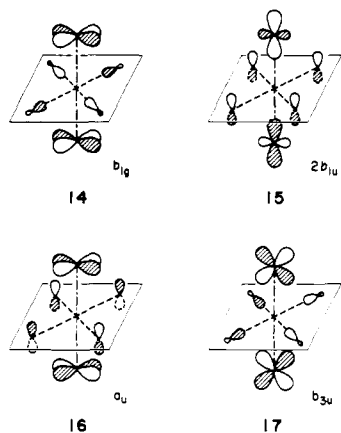


**Figure 3.** Interaction diagram for the valence orbitals of  $[\text{Rh}(\text{CO})_2]_2\text{N}_4$ . At right, two  $\text{Rh}(\text{CO})_2^+$  fragments are combined, held in a  $D_{2h}$  geometry. Then the  $[\text{Rh}(\text{CO})_2]_2^{2+}$  composite is mixed with  $(\text{NH}_2)_4^{4-}$  at left.

( $xz$ ),  $1a_2$  ( $xy$ ), and  $2a_1$  ( $x^2 - y^2$ ) in local  $C_{2v}$  symmetry. These lower d block orbitals are fully occupied for  $\text{Rh}(\text{CO})_2^+$ . In the two higher vacant levels, Rh d orbitals are hybridized with Rh p's in such a way that orbital lobes point away from the two carbonyl ligands. A weakly interacting  $[\text{Rh}(\text{CO})_2]_2^{2+}$  pair provides bonding and antibonding combinations of each valence orbital of the  $\text{Rh}(\text{CO})_2$  fragment. On being allowed to interact with the  $\text{N}_4$  orbitals, the valence levels of the  $[\text{Rh}(\text{CO})_2]_2^{2+}$  composite are all pushed up by different amounts. Among the eight occupied d orbital combinations, the  $b_{3u}$ ,  $b_{1g}$ ,  $b_{1u}$ , and  $a_u$  are strongly destabilized. The  $b_{1g}$  and the  $a_u$  comprise in-phase and out-of-phase combinations of  $xy$  orbital components, while the  $b_{3u}$  has an in-phase  $xz$  combination. The  $x^2 - y^2$  and  $z^2$  orbital pairs are mixed with each other in the two  $b_{1u}$  levels, and the higher  $2b_{1u}$  is destabilized. These four levels are sketched in 14–17.



The skewing deformation of  $[\text{Rh}(\text{CO})_2]_2\text{OEP}$  has two aspects. One is a slipping of the  $\text{Rh}(\text{CO})_2$  units off the points above and below the center of the porphyrin, while the other is a tilting of the  $\text{Rh}(\text{CO})_2$  planes. We describe the two components of the deformations by the two geometrical var-

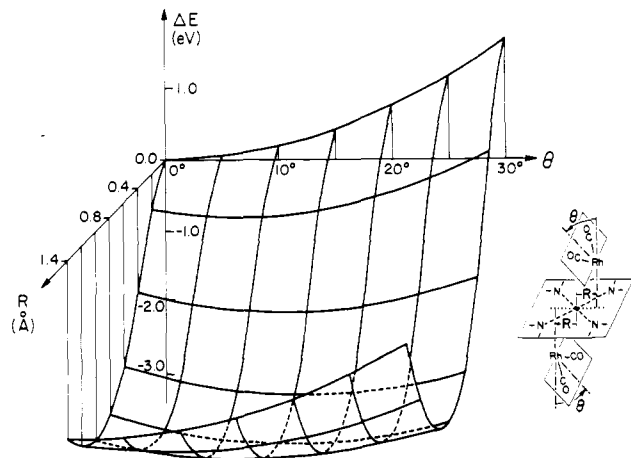
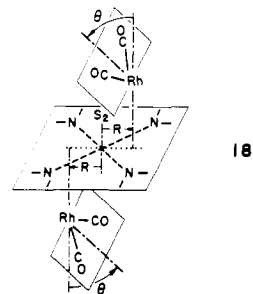


**Figure 4.** Potential energy surface for slipping ( $R$ ) and bonding ( $\theta$ ) deformations of the  $\text{Rh}(\text{CO})_2$  groups above and below the  $\text{N}_4$  plane. The energies are in electron volts relative to the nondeformed geometry ( $R = 0.0 \text{ \AA}$ ,  $\theta = 0^\circ$ ).

iables  $R$  and  $\theta$ , as shown in 18. All other geometrical pa-



rameters are kept fixed. The computed total energy surface as a function of  $R$  and  $\theta$  (Figure 4) is interesting. Stabilization of the molecule is achieved primarily by the slipping mode—the potential valley locates around  $R = 0.8 \text{ \AA}$ .

A Walsh diagram for the slipping, not presented here, allows one to trace the deformation once again to a “release of antibonding interaction”, similar to the reasoning used for  $[\text{Re}(\text{CO})_3]_2\text{TPP}$ . In particular, the main contributors are  $1b_{1g}$  (14), and  $1a_u$  (16), analogous to  $2a_g$  and  $2b_u$  of  $[\text{Re}(\text{CO})_3]_2\text{N}_4$ , respectively.

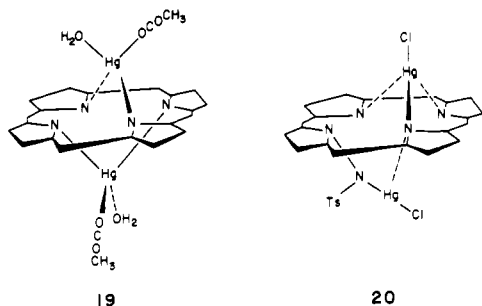
The effect of  $\text{Rh}(\text{CO})_2$  tilting on the total energy (Figure 4) is interesting. Whether the tilting ( $\theta$ ) is stabilizing or not depends on the extent of slipping ( $R$ ).

When the Rh atoms still sit on the  $S_2$  axis ( $R = 0.0 \text{ \AA}$ ) or when the  $\text{Rh}(\text{CO})_2$  units are moved far off the axis ( $R = 1.4 \text{ \AA}$ ), the tilting deformation costs energy. The point in which the tilting is the most effective in stabilizing the molecule is at  $R = 0.8 \text{ \AA}$ . The computed potential minimum comes at  $\theta = 16^\circ$ , while the observed angle is  $\theta \approx 26^\circ$ . The tilting and slipping deformations together produce an approximately square-planar (two porphyrin nitrogens, two carbonyls) local coordination at each Rh. This coordination geometry, of course, is typical of  $d^8$  four-coordinate complexes.

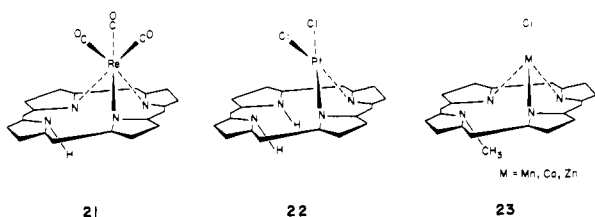
Is there any metal-metal bonding, “through the porphyrin”, in these complexes? From the interaction diagrams (Figures 1 and 3), one can see that both bonding and antibonding combinations of  $\sigma$ ,  $\pi$ , and  $\delta$  pseudosymmetry are occupied. Thus no strong metal-metal bonding can be anticipated. The computed M–M overlap populations are 0.048 and 0.118 for the nonskewed  $[\text{Re}(\text{CO})_3]_2\text{N}_4$  and  $[\text{Rh}(\text{CO})_2]_2\text{N}_4$ , respectively. These numbers drop to 0.016 and 0.018 when the molecules are deformed ( $R = 0.8 \text{ \AA}$ ). Such small numerical values are indicative of little, if any, metal-metal bonding.

Are there any other  $(\text{ML})_2(\text{porphyrin})$  complexes for which slipping might be expected? An interesting molecule is the

novel bis(mercury(II)) porphyrin structure which has been assigned to the compound  $[\text{Hg}(\text{OCOCH}_3)(\text{H}_2\text{O})]_2\text{TPP}$  **19**.<sup>8</sup>

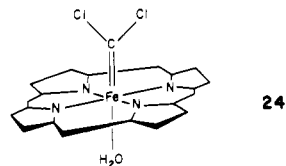


The lack of an X-ray diffraction study on the molecule, however, does not allow us to judge whether the molecule has a slipped geometry. The complex structure of bis(chloro-mercury(II))-*N*-tosylamino-OEP **20**<sup>9</sup> is available. Perhaps not unrelated to the skewed  $[\text{ML}_n]_2(\text{porphyrin})$  are those complexes in which a small fragment such as H, "2H", or CH<sub>3</sub> replaces one of the metal components. Examples are the structures assigned to  $\text{H}[\text{Re}(\text{CO})_3]\text{TPP}$ <sup>2a</sup> **21** and *cis*-



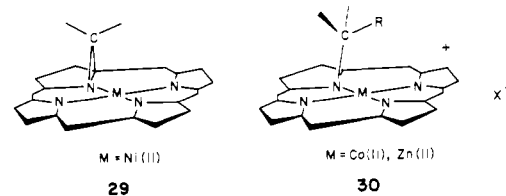
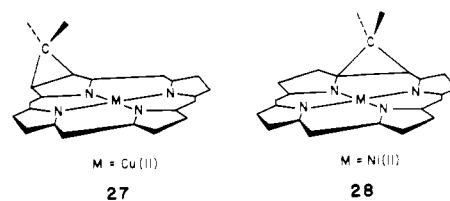
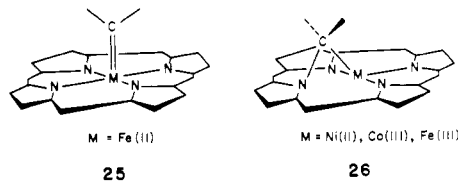
$\text{PtCl}_2\text{H}_2$ (hematoporphyrin) **22**<sup>10</sup> and those determined for a series of *N*-methyl-TPP complexes with Mn(II), Co(II), and Zn(II) **23**.<sup>11</sup> Given the synthetic success of the isolobal analogy,<sup>12</sup> we expect that the future will bring us a multitude of  $(\text{CpM})_2$ ,  $(\text{CpML})_2$ , and  $(\text{CpML}_2)_2(\text{porphyrin})$  complexes.

**Carbene Complexes of Metalloporphyrins.** The appearance of a carbene as an axial metalloporphyrin ligand is a relatively recent phenomenon. The first isolated carbene metalloporphyrin complexes were  $\text{Fe}(\text{TPP})(\text{CCl}_2)$  and  $\text{Fe}(\text{TPP})(\text{C}-\text{Cl}_2)(\text{L})$ , synthesized by the reaction of  $\text{Fe}(\text{TPP})$  with  $\text{CCl}_4$  in the presence of an excess of reducing agent.<sup>13a</sup> A crystal structure is available for  $\text{Fe}(\text{TPP})(\text{CCl}_2)(\text{H}_2\text{O})$ , in which the plane defined by the Fe, C, and two Cl atoms is practically perpendicular to the mean plane of the porphyrin, **24**.<sup>13b</sup> Other carbene complexes available include  $\text{Fe}(\text{porphyrin})-[\text{C}=\text{C}(\text{C}_8\text{H}_4\text{Cl})_2]$  (porphyrin = TPP, *p*-Me(TPP), *p*-Cl(TPP), OEP, protoporphyrin IX),  $\text{Fe}(\text{TPP})(1,3\text{-benzodioxal-2-carbene})$ , and  $\text{Fe}(\text{TPP})(\text{CClX})$  (X = CN and  $\text{COOC}_2\text{H}_5$ ).<sup>13c</sup> Evidence has also been reported for the formation of a cyto-



chrome P450 iron-carbene complex during the reductive metabolism of polyhalogenated compounds.<sup>14</sup>

Coordination to the central metal **25** is not the one and only geometrical choice available to a carbene fragment in a metalloporphyrin. The carbene may be inserted into a metal-nitrogen bond **26** or may add to the  $\beta\beta$  partial double bond **27**.<sup>15</sup> When heated to 140 °C, **26** rearranged to the homoporphyrinato derivatives **28**, possibly through an aziridine, i.e.,



an adduct of carbene to an N-C bond, **29**.<sup>17</sup> Aziridine **29** is also generated from the *N*-alkyl metalloporphyrin **30**, which is a reduction product from **26**, when treated with base.<sup>17,18</sup> For a longer reaction period with base, **29** then turns to **26**.<sup>16</sup> Demetalated compounds of **30** react with metal ions, yielding **28**.<sup>17,19</sup> The central metal of all these isomers occasionally takes up another axial ligand.<sup>20</sup>

These lovely reaction sequences show that there are many possible sites for a carbene fragment interacting with a metalloporphyrin. Fluxional behavior for a carbene molecule atop a metalloporphyrin plane is not surprising, if we recognize the large delocalized  $\pi$ -electron system awaiting an electron-deficient carbene fragment. Our present analysis regrettably is restricted to a piece of the complete surface, the transformation

- (8) Hudson, M. F.; Smith, K. M. *Tetrahedron Lett.* **1974**, 2223-2226.  
 (9) Callot, H. J.; Chevri er, B.; Weiss, R. *J. Am. Chem. Soc.* **1979**, *101*, 7729-7730.  
 (10) Anderson, O. P.; Lavallee, D. K. *J. Am. Chem. Soc.* **1976**, *98*, 4670-4671; **1977**, *99*, 1404-1499; *Inorg. Chem.* **1977**, *16*, 1634-1640. Lavallee, D. K.; Kopelove, A. B.; Anderson, O. P. *J. Am. Chem. Soc.* **1978**, *100*, 3025-3033.  
 (11) Macquet, J. P.; Millard, M. M.; Theophanides, T. *J. Am. Chem. Soc.* **1978**, *100*, 4741-4746.  
 (12) Lauher, J. W.; Elian, M.; Summerville, R. H.; Hoffmann, R. *J. Am. Chem. Soc.* **1976**, *98*, 3219-3224. Elian, M.; Chen, M. M. L.; Mingos, D. M. P.; Hoffmann, R. *Inorg. Chem.* **1976**, *15*, 1148-1155. Pinhas, A. R.; Albright, T. A.; Hofmann, P.; Hoffmann, R. *Helv. Chim. Acta* **1980**, *63*, 29-43.  
 (13) (a) Mansuy, D.; Lange, M.; Chottard, J.-C.; Guerin, P. *J. Chem. Soc., Chem. Commun.* **1977**, 648-649. (b) Mansuy, D.; Lange, M.; Chottard, J.-C.; Bartoli, J. F.; Chevri er, B.; Weiss, R. *Angew. Chem., Int. Ed. Engl.* **1978**, *17*, 781-782. (c) Mansuy, D.; Lange, M.; Chottard, J. C. *J. Am. Chem. Soc.* **1978**, *100*, 3213-3214. Mansuy, D.; Battioni, J.-P.; Chottard, J.-C.; Ullrich, V. *Ibid.* **1979**, *101*, 3971-3973. Mansuy, D.; Guerin, P.; Chottard, J.-C. *J. Organomet. Chem.* **1979**, *171*, 195-201.

- (14) (a) Nastainczyk, N.; Ullrich, V.; Sies, H. *Biochem. Pharmacol.* **1978**, *27*, 387-390 and references therein. (b) Uehleke, H.; Hellmer, K. H.; Tabarelli-Poplawski, S. *Arch. Pharm. (Weinheim, Ger.)* **1973**, *279*, 39-52.  
 (15) Callot, H. J.; Johnson, A. W.; Sweeney, A. *J. Chem. Soc., Perkins Trans. 1* **1973**, 1424-1427.  
 (16) Callot, H. J.; Tschamber, Th.; Chevri er, B.; Weiss, R. *Angew. Chem., Int. Ed. Engl.* **1975**, *14*, 567-568.  
 (17) Callot, H. J.; Tschamber, Th. *Tetrahedron Lett.* **1974**, 3155-3158, 3159-3162.  
 (18) Callot, H. J.; Tschamber, Th. *Bull. Soc. Chim. Fr.* **1973**, 3192-3198.  
 (19) Chevri er, B.; Weiss, R. *J. Chem. Soc., Chem. Commun.* **1974**, 884-885; *J. Am. Chem. Soc.* **1975**, *97*, 1416-1421.  
 (20) (a) The reaction sequences are discussed in: Callot, H. J.; Schaeffer, E. *Nouv. J. Chim.* **1980**, *4*, 307-309. (b) Callot, H. J.; Tschamber, Th. *J. Am. Chem. Soc.* **1975**, *97*, 6175-6178. (c) Callot, H. J.; Schaeffer, E. *Tetrahedron* **1978**, *34*, 2295-2300; *Tetrahedron Lett.* **1980**, *21*, 111-115.

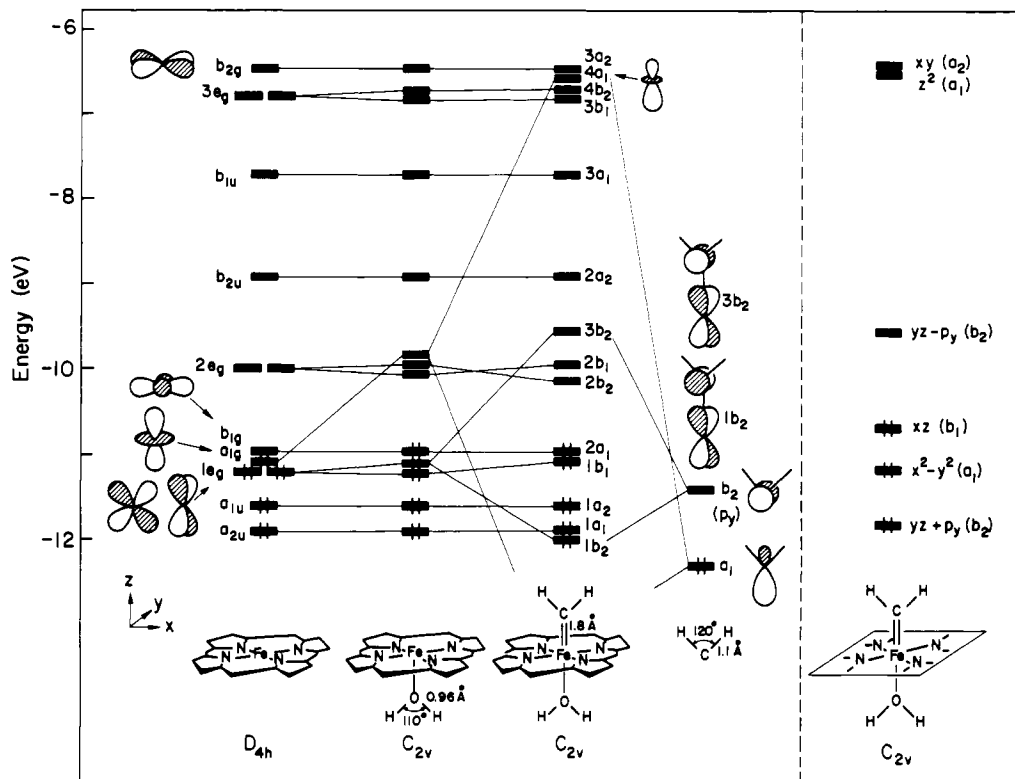
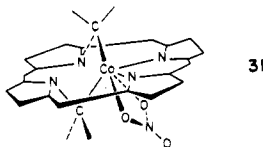


**Figure 5.** Interaction diagram for the valence orbitals of  $\text{Fe}(\text{porphyrin})(\text{OH}_2)(\text{CH}_2)$  (to the left of the dashed line). From left to right: the orbitals of  $\text{Fe}(\text{porphyrin})$ ; square-pyramidal  $\text{Fe}(\text{porphyrin})(\text{OH}_2)$  in which an  $\text{H}_2\text{O}$  molecule occupies an axial coordination site at  $\text{Fe}$  ( $\text{Fe}-\text{O} = 2.13 \text{ \AA}$ ); the orbitals of the carbene complex; the  $\text{CH}_2$  orbitals. To the right of the dashed line are the valence orbitals of the model carbene complex  $\text{Fe}(\text{N}_4)(\text{OH}_2)(\text{CH}_2)$ .

of **25** and **26**. So far only  $\text{Fe}(\text{II})$ , with a  $d^6$  electron count,<sup>21</sup> has been found to form stable carbene complexes of type **25**. On the other hand, the carbene-inserted products of type **26** are more variegated. X-ray crystallographic studies are available for  $d^5$   $\text{Fe}(\text{TPP})\text{Cl}(\text{C}=\text{CAR}_2)$ <sup>22</sup> and  $d^8$   $\text{Ni}(\text{TPP})(\text{CHCOOEt})$ .<sup>16,23</sup> For  $d^6$   $\text{Co}(\text{III})$ , the compounds isolated and characterized include  $[\text{Co}(\text{OEP})(\text{CHCOOEt})]^+\text{Cl}^-$ <sup>24</sup> and  $[\text{Co}(\text{TPP})(\text{CHCOOEt})]^+\text{Cl}^-$ .<sup>25</sup> A 1:2 adduct of cobalt(III) porphyrin and ethoxycarbonyl carbenes  $\text{Co}(\text{OEP})(\text{CHCOOEt})_2(\text{NO}_3)$  is also available, the structure of which is shown in **31**. What are the factors which influence the choice of structure **25** or **26**?



First we explore the basic pattern of bonding between a carbene and a central metal in a metalloporphyrin.<sup>26,27</sup> We have calculated the electronic structures of  $\text{Fe}(\text{porphyrin})-$

$(\text{OH}_2)(\text{CH}_2)$  and the simplified molecule  $\text{Fe}(\text{N}_4)(\text{OH}_2)(\text{CH}_2)^{2-}$ , which are the models for  $\text{Fe}(\text{TPP})(\text{OH}_2)(\text{CCl}_2)$ . Note our use of the full porphyrin ring as well as the  $\text{N}_4$  model. Molecular orbitals of  $\text{Fe}(\text{porphyrin})(\text{OH}_2)(\text{CH}_2)$  are constructed in Figure 5. Bond distances,  $1.8 \text{ \AA}$  for  $\text{Fe}-\text{C}$  and  $2.13 \text{ \AA}$  for  $\text{Fe}-\text{O}$ , were taken from those in  $\text{Fe}(\text{TPP})(\text{O}-\text{H}_2)(\text{CCl}_2)$ .<sup>13b</sup>  $\text{CH}_2$  and  $\text{H}_2\text{O}$  are eclipsed to each other and staggered with respect to the porphyrin nitrogen atoms.

At the left of Figure 5 there are 12 frontier molecule orbitals of  $\text{Fe}(\text{porphyrin})$ ; five of them comprise  $\text{Fe}$  d orbitals and others, some of porphyrin  $\pi$  orbitals. In the  $D_{4h}$  square-planar geometry, the d levels split in such a manner that four low-lying levels  $x^2 - y^2$  ( $b_{1g}$ ),  $z^2$  ( $a_{1g}$ ),  $xz$  and  $yz$  ( $1e_g$ ) are very close to each other and  $xy$  ( $b_{2g}$ ) is alone at high energy. The coordination of a  $\sigma$ -donor  $\text{H}_2\text{O}$  pushes up the  $z^2$  energy level. One of  $d_\pi$  orbitals,  $yz$ , also moves up, only slightly so, because the  $\pi$ -donor ability of  $\text{H}_2\text{O}$  is so small. In the fourth column of the figure, we have  $\text{CH}_2$  carrying two frontier orbitals, the  $\sigma$ -donor and the p-acceptor orbitals. These interact strongly with  $\text{Fe}$   $z^2$  and  $yz$ . Most of the metal-carbene  $\sigma$  and  $\pi$  bonding is achieved through these interactions. Other d orbitals,  $x^2 - y^2$  and  $xz$ , remain nonbonding. Interestingly, the porphyrin  $\pi$  orbitals are nearly innocent of interaction, retaining their original energies in  $\text{Fe}(\text{porphyrin})$ .

The frontier orbitals of the simplified model  $\text{Fe}(\text{N}_4)(\text{O}-\text{H}_2)(\text{CH}_2)$  are given at the extreme right of Figure 5. The orbital diagram, of course, does not contain any orbitals corresponding to the porphyrin  $\pi$  orbitals of  $\text{Fe}(\text{porphyrin})(\text{OH}_2)(\text{CH}_2)$ . However, the pattern of d level splittings of  $\text{Fe}(\text{porphyrin})(\text{OH}_2)(\text{CH}_2)$  is preserved very well in the  $\text{N}_4$  model. The strong  $\text{Fe}-\text{CH}_2$   $\sigma$  interaction leaves the  $\sigma^*$  level as high as  $xy$  in energy. A somewhat weaker  $\pi$  interaction gives a relatively low  $\pi^*$  level which is made up of 50% of  $yz$  and 43% of the C(carbene)  $p_y$  orbitals. Nonbonding  $x^2 - y^2$  and  $xz$  orbitals sit in between the  $\pi-\pi^*$  pair. The quite good agreement between d-energy level patterns gives us confidence

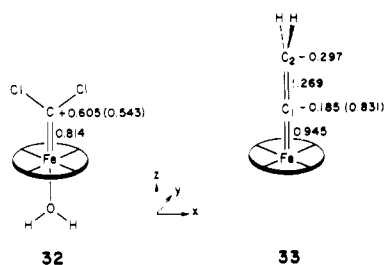
- (21) A carbene ligand is viewed as neutral in our electron count convention.  
 (22) Mansuy, D., private communication.  
 (23) Chevrier, B.; Weiss, R. *J. Am. Chem. Soc.* **1976**, *98*, 2985-2990.  
 (24) Batten, P.; Hamilton, A.; Johnson, A. W.; Shelton, G.; Ward, D. *J. Chem. Soc., Chem. Commun.* **1974**, 550-551. Johnson, A. W.; Ward, D.; Batten, P.; Hamilton, A.; Shelton, G.; Elson, C. M. *J. Chem. Soc., Perkin Trans. 1* **1975**, 2076-2085.  
 (25) Johnson, A. W.; Ward, D. *J. Chem. Soc., Perkin Trans. 1*, **1977**, 720-723.  
 (26) Other molecular orbital calculations for transition-metal carbene complexes are presented in the following papers: (a) Block, T. F.; Fenske, R. F.; Casey, C. P. *J. Am. Chem. Soc.* **1976**, *98*, 441-443. (b) Goddard, R. J.; Hoffmann, R.; Jemmis, E. D. *Ibid.* **1980**, *102*, 7667-7676.  
 (27) A model carbene P450 complex,  $\text{Fe}(\text{porphyrin})(\text{CHCF}_3)(\text{SCH}_3)$ , has been calculated by the INDO method in order to assign the electronic spectra: Loew, G.; Goldblum, A. *J. Am. Chem. Soc.* **1980**, *102*, 3657-3659.

in the reliability of the simplest  $N_4$  model for a large porphyrin ring, at least for ground-state properties.

Fe(porphyrin)(OH<sub>2</sub>)(CH<sub>2</sub>) as well as the existing molecule Fe(TPP)(OH<sub>2</sub>)(CCl<sub>2</sub>) is a  $d^6$  electron system. Thus the highest occupied level is a nonbonding  $d$  orbital,  $x^2 - y^2$  or  $xz$ . The Fe-CH<sub>2</sub>  $\sigma^*$  and  $\pi^*$  levels are both unoccupied, so that the Fe-C bond is expected to have double-bond character. In fact the X-ray diffraction data of Fe(TPP)(OH<sub>2</sub>)(CCl<sub>2</sub>) show a short Fe-C bond length (1.83 Å). Now suppose we have a  $d^8$  system, with two extra electrons. In Figure 5 those two electrons would enter a porphyrin  $\pi$  orbital ( $2b_2$ ). However, we think it is more likely that in reality they enter the  $M=CH_2$   $\pi^*$  level ( $3b_2$ ), and this is supported by computations on a model  $d^8$  Ni(porphyrin)(CH<sub>2</sub>). Occupation of  $\pi^*$  is important because it implies disruption of  $M=CH_2$  double bonding. In fact, in the case of  $d^8$  Ni(porphyrin)(CHCOOC<sub>2</sub>H<sub>5</sub>), the carbene sits above a point between Ni and one of four N atoms in a porphyrin ring (structure **26**).

Thus the number of  $d$  electrons is one important factor governing the geometrical choice between **25** and **26**. Had we only the Fe(TPP)(OH<sub>2</sub>)(CCl<sub>2</sub>) and Ni(TPP)(CHCOOC<sub>2</sub>H<sub>5</sub>) structures in hand, we would be satisfied with our explanations. However, nature is not always so obedient to simplistic theories. Although there is no example of  $d^8$  carbene-metalloporphyrin complex of type **25**, the  $d^6$  electron count is not a sufficient condition to guarantee that structure. The aforementioned Co(III) complexes [Co(OEP)-(CHCOOEt)]Cl, [Co(TPP)(CHCOOEt)]Cl, and Co(OEP)(CHCOOEt)<sub>2</sub>(NO<sub>3</sub>) are all  $d^6$  but prefer **26** to **25**.

We will deepen our analysis of this geometrical preference soon. Before going further, we comment on some chemical characteristics of the Fe=C(carbene) bond in porphyrin complexes. The Fe-C overlap populations, charges on the carbon atoms, and carbon  $2p_y$  populations have been calculated for Fe(porphyrin)(OH<sub>2</sub>)(CCl<sub>2</sub>) and Fe(porphyrin)(C=CH<sub>2</sub>),<sup>28</sup> which are models for the well-characterized carbene complexes Fe(TPP)(OH<sub>2</sub>)(CCl<sub>2</sub>) and Fe(TPP)(C=CAr<sub>2</sub>). The calculated values are given in **32** and **33** where the signed numbers

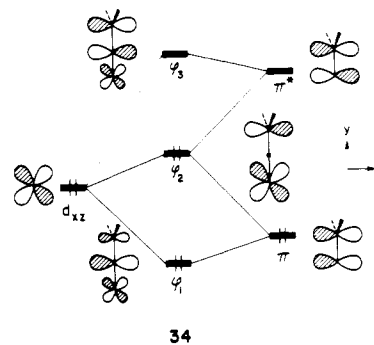


are carbon charges and the numbers in parentheses are  $2p_y$  populations. The Fe-C overlap populations are large, compared with those of M-C(alkyl) single bonds which usually range from around 0.4 to 0.5 in extended Hückel calculations. The charge on the carbene carbon atom of Fe(porphyrin)(OH<sub>2</sub>)(CCl<sub>2</sub>) is highly positive (+0.605). In part this is due to  $\sigma$ -electron drift to the electronegative Cl substituents (calculated carbon charge in a free carbene, CCl<sub>2</sub>, is +0.310), but there is also greater CCl<sub>2</sub>  $\rightarrow$  Fe  $\sigma$  donation of electrons than Fe  $\rightarrow$  CCl<sub>2</sub>  $\pi$  back-donation. The electropositive nature of the carbene carbon may be relevant to the experimental fact<sup>13b</sup> that good nucleophiles such as primary amines, phosphines, and thiolates rapidly destroy the Fe-CCl<sub>2</sub> bond of Fe(TPP)(CCl<sub>2</sub>). The decomposition of the compound by

primary amines RNH<sub>2</sub> gives isocyanides RNC. Fe(TPP)(C-Cl<sub>2</sub>) is also slowly oxidized in aerated solvents.

For the vinylidene carbene complex **33**, the Fe=C<sub>1</sub> overlap population is slightly larger than that for the dichlorocarbene complex **32**. The most striking aspect of the population analysis of **33** is, however, the negative charge on the carbene carbon C<sub>1</sub>, which contrasts with the large positive charge on the corresponding carbon in **32**. C<sub>1</sub> does have more electrons in its  $2p_y$  orbital than **32**. These two criteria of carbon charge and carbon  $2p_y$  population<sup>26b</sup> indicate stronger nucleophilicity or weaker electrophilicity of **33** at the C<sub>1</sub> site, relative to **32**. There is so far no experimental evidence pointing to nucleophilic character for Fe(TPP)C=CAr<sub>2</sub>). However, it may be noted that Fe(TPP)(C=CAr<sub>2</sub>) is remarkably stable in aerated solvents, while Fe(TPP)(OH<sub>2</sub>)(CCl<sub>2</sub>) is oxidized with a half-life of 4 h under the same conditions.<sup>13c</sup>

Much of the difference between the methylene and vinylidene complex electron distributions may be traced to the second  $\pi$  system of **33**. Interaction between C<sub>1</sub>-C<sub>2</sub>  $\pi$  and  $\pi^*$  and Fe  $d_{xz}$  yields a set of typical allylic type orbitals,  $\varphi_1$ ,  $\varphi_2$ ,  $\varphi_3$ , as shown in **34**.<sup>29,30</sup> In the  $d^6$  Fe(porphyrin)(C=CH<sub>2</sub>),



the HOMO is actually  $\varphi_2$ . This simple interaction diagram contains the following information. (1) The occupied  $\varphi_1$  orbital provides a net Fe  $d_{xz}$ -C<sub>1</sub>  $p_x$  bonding interaction, thus increasing the Fe-C<sub>1</sub> bond strength. The calculated  $d_{xz}$ - $p_x$  overlap population amounts to 0.108. This is the main reason that the Fe-C<sub>1</sub> total overlap population of **33** is larger than that of **32**.

(2) As a consequence of the delocalization of the  $\varphi_1$  orbital over three centers, the C<sub>1</sub>-C<sub>2</sub>  $\pi$  bond in **33** is weakened relative to a free vinylidene carbene C=CH<sub>2</sub>. This would result in an elongation of the C<sub>1</sub>-C<sub>2</sub> bond in the iron porphyrin complex. Our model calculations show that the C<sub>1</sub>  $p_x$ -C<sub>2</sub>  $p_x$  and total C<sub>1</sub>-C<sub>2</sub> overlap populations drop from 0.420 and 1.340 for :C=CH<sub>2</sub> to 0.360 and 1.269 for Fe(porphyrin)(C=CH<sub>2</sub>), respectively.

(3) Occupation of  $\varphi_2$  by two electrons polarizes the  $\pi$ -electron distribution in such a way that the terminal carbon atom, C<sub>2</sub>, carries more  $\pi$  electrons than C<sub>1</sub>.<sup>30</sup> Accordingly, the calculated  $p_x$   $\pi$ -electron density is larger for C<sub>2</sub>, 1.255, than for C<sub>1</sub>, 0.960.

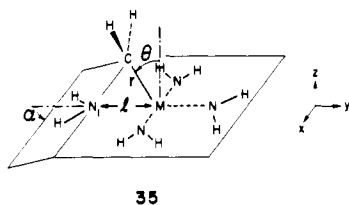
Now let us return to the carbene-coordination **25** vs. carbene-insertion **26** problem. The insertion pathway is complex—it involves not only a shift of the carbene fragment but also a deformation of the porphyrin ring. We turned to the  $N_4$  model and varied four geometrical parameters. These were the M-C distance  $r$ , the M-N<sub>1</sub> distance,  $l$ ,  $z$ -M-C angle

(28) Geometrical parameters employed are as follows: for [Fe(porphyrin)(CCl<sub>2</sub>)(OH<sub>2</sub>)], Fe-C 1.83 Å, C-Cl 1.76 Å, Fe-O 2.13 Å, O-H 0.96 Å, Cl-C-Cl 120°, and H-O-H 105°; for [Fe(porphyrin)(C=CH<sub>2</sub>)], Fe-C 1.80 Å, C-C 1.35 Å, and H-C-H 120°. In both model compounds, Fe sits in the middle of the porphyrin ring.

(29) The allylic type orbitals of M-X-Y  $\pi$  systems have been discussed by us in: Hoffmann, R.; Chem. M. M.-L.; Thorn, D. L. *Inorg. Chem.* **1977**, *16*, 503-511.

(30) This polarization has been noted in: Johnson, J. B.; Klemperer, W. G. *J. Am. Chem. Soc.* **1977**, *99*, 7132-7137. Demuyneck, J.; Veillard, A. *Theoret. Chim. Acta* **1973**, *28*, 241-265.

$\theta$ , and  $N_1H_2$  bending angle  $\alpha$  (35). Other geometrical pa-



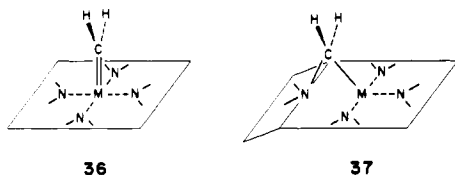
35

rameters were kept constant; for instance, the C atom is located always above a point between M and  $N_1$ , and the  $CH_2$  plane is kept parallel to the  $xz$  plane. Note that in this calculation the coordinate system is the same as that in Figure 5 and 32, as far as the carbene is concerned, but the porphyrin is rotated by  $45^\circ$ .

From the introduction to this section it will be recalled that it was not only the d electron count but also the nature of the metal which determined the choice of geometry. To explore this we have calculated total energy curves along the hypothetical pathway for  $M(N_4)(CH_2)$  in which M carries Ni orbitals but with a variable 3d orbital energy,  $-14.0$  to  $-11.5$  eV. Figure 6 shows potential curves for two electronic configurations,  $d^6$  and  $d^8$ , of  $M(N_4)(CH_2)$ .

A common feature of the computed potential curves in Figure 6 is the presence of two local minima, one at  $\theta = 0^\circ$  (36) and the other at  $\theta = 48-64^\circ$  (37). The former minimum clearly is for a geometry corresponding to a metal-carbene complex 25, while the latter corresponds to a carbene-inserted compound 26. Noticeable is the rather flat potential curve for the  $d^6$  system. Thus the stable geometry of the  $d^6$  molecules might be very sensitive to a small variation in electronic properties of the central metal, a carbene fragment, and/or an additional axial ligand if it is present.

For a given d orbital energy, the stability of 37 relative to 36 is increased, or the relative stability of 36 is decreased, on



36

37

going from  $d^6$  to  $d^8$ . This result supports the interpretation, given earlier in this section, in an attempt to rationalize the geometry of  $d^8$  Ni(TPP)(CHCOOC<sub>2</sub>H<sub>5</sub>). Occupancy of two electrons in the M-C(carbene)  $\pi^*$  level is the reason that the  $d^8$  molecule tends to geometry 37 rather than 36.

The energy of the d orbital levels, i.e., the electronegativity of the metal, is also an important factor in determining the geometry. A lower positioning of the d energy levels increases the relative stability of 37, notably for  $d^8$ . Our Ni(II) parameters, which were obtained by charge iterative calculations on the model  $Ni^{II}(N_4)^{2-}$ , place the Ni 3d energy as low as  $-13.49$  eV. Thus  $Ni^{II}(\text{porphyrin})(\text{carbene})$  is a case in which both the  $d^8$  electron count and the low d orbital energy make the geometry 37 more stable.

The most striking aspect of the potential energy curves of Figure 6 is that the  $d^6$  molecule does *not* always prefer the simple carbene adduct to the inserted product. When the d levels are high in energy, 36 is still the more stable geometry. However, the lowering of the d energy moves the system from 36 to 37. This must be the main reason that the carbene fragment of  $d^6$   $Co^{III}(\text{porphyrin})(\text{CHCOOEt})^+$  tends to be inserted into a Co-N bond while  $d^6$   $Fe^{II}(\text{TPP})(\text{CCl}_2)(\text{H}_2\text{O})$  forms an Fe=C double bond. With our parameters, the Fe(II) 3d energy level is placed at  $-11.46$  eV and Co(III) 3d at  $-13.31$  eV. We have calculated hypothetical potential curves for  $Fe^{II}(N_4)(CH_2)^{2-}$  and  $Co^{III}(N_4)(CH_2)^{2-}$ , where we used the

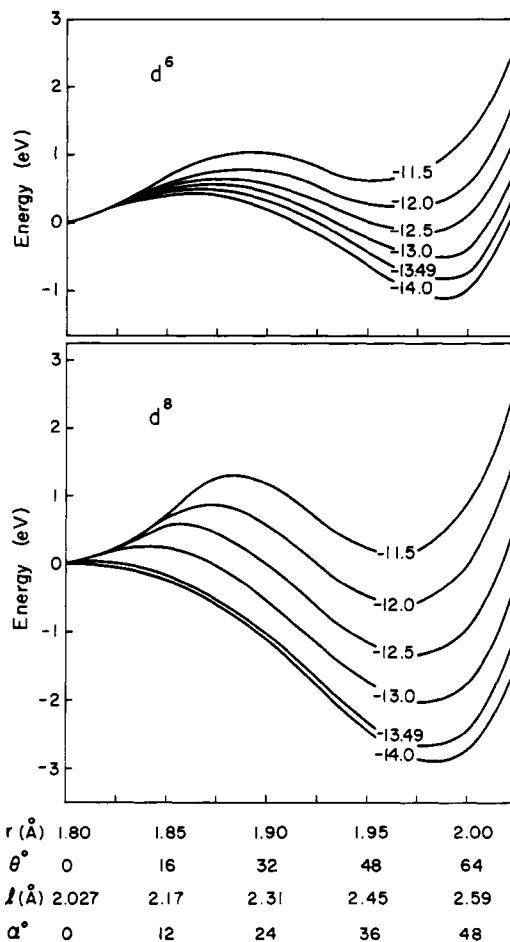


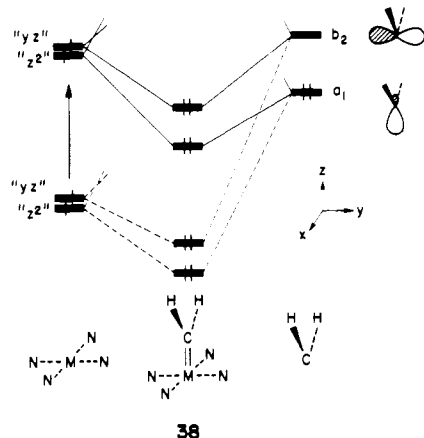
**Figure 6.** Total energy curves along the hypothetical insertion pathway for two electronic configurations of  $M(N_4)(CH_2)$ ;  $d^6$  (top) and  $d^8$  (bottom). The geometrical parameters defining the pathway are shown in 35. The metal atom M carries Ni orbitals with a variable 3d orbital energy,  $-14.0$  to  $-11.5$  eV. Potential curves for various choices of the Ni 3d energy are superimposed in such a way that all curves are referred to an arbitrary zero of energy at  $r = 1.80$  Å,  $\theta = 0^\circ$ ,  $l = 2.027$  Å, and  $\alpha = 0^\circ$ .

same geometrical variables as those defined in Figure 6. For  $Fe^{II}(N_4)(CH_2)^{2-}$ , as one could expect, geometry 36 ( $\theta = 0^\circ$ ,  $\alpha = 0^\circ$ ,  $r = 1.80$  Å,  $l = 2.027$  Å) is 2.2 eV more stable than another potential minimum at  $\theta = 48^\circ$ ,  $\alpha = 36^\circ$ ,  $r = 1.80$  Å, and  $l = 2.45$  Å. On the other hand,  $Co^{III}(N_4)(CH_2)^-$  finds its stable geometry at  $\theta = 56^\circ$ ,  $\alpha = 42^\circ$ ,  $r = 1.975$  Å, and  $l = 2.52$  Å, which is 0.1 eV more stable than 36. Although we should not rely on these numbers in a quantitative sense, the contrast between the potential curves for Fe(II) and Co(III) is significant.

Let us try to understand the effect of the d orbital on the relative stability of 36 and 37. First consider the  $d^6$  molecule of the structure 36. We know from Figures 5 and 6 that the " $z^2$ "- $\sigma(a_1)$  and " $yz$ "- $\pi(b_2)$  interactions govern stability (and strength) of the M=C(carbene) double bond. If we vary the metal d energy  $H_{ii}(d)$ , then there are two effects to be considered. One is the amount of admixture of  $N_4$  orbitals in to the  $M(N_4)$  " $z^2$ " and " $yz$ " orbitals. This is a sort of secondary effect on the M=C bond strength but cannot be ignored. A smaller admixture of  $N_4$  orbitals, which in turn leads to a larger proportion of M  $z^2$  and  $yz$  in the  $M(N_4)$  orbitals, results in a greater M=C local overlap interaction. Since the  $N_4$  energies are set low, a higher d orbital positioning always yields " $z^2$ " and " $yz$ " with larger d components. Thus, as far as this secondary effect is concerned, the M-C interaction is increased when the d energy is raised.



The other effect is more straightforward, i.e., " $z^2$ "- $\sigma$  and " $yz$ "- $\pi$  energy separations. A stronger M=C covalent bond is formed when the " $z^2$ " and " $yz$ " energies of  $M(N_4)$  come closer to the  $\sigma$  and  $\pi$  energies of  $CH_2$ , respectively. This is shown schematically in **38**. In our extended Hückel calcu-



lations, the  $\sigma$  ( $a_1$ ) is placed at  $-12.3$  eV and the  $\pi$  ( $b_2$ ) at  $-11.4$  eV. If  $H_{ii}(d)$  is varied from  $-14.0$  to  $-11.5$  eV, the " $z^2$ " and " $yz$ " energies of  $M(N_4)$  move from  $-14.3$  and  $-13.7$  eV to  $-11.4$  and  $-11.3$  eV, respectively.

As a consequence of the two effects, the stability of the M=C bond (thus of geometry **36**) increases monotonically with higher M d energy. This must be what is behind the behavior of  $d^6$  potential curves in Figure 6. The trend may be followed by observing the M-C overlap population, which increases constantly from 0.480 for  $H_{ii}(d) = -14.0$  eV to 0.685 for  $H_{ii}(d) = -11.5$  eV. Our reasoning is based only on the electronic structure of the molecule **36** and lacks an analysis of the alternative carbene-inserted geometry **37**. We think, however, that the bonding in **37** is less sensitive to a d energy change compared with that in **36**. In fact the sum of the N-C and C-M overlap populations in **37** is almost unchanged, being 1.12 for  $H_{ii}(d) = -14.0$  eV and 1.16 for  $H_{ii}(d) = -11.5$  eV. Reasoning along similar lines, one can rationalize the shape of the  $d^8$  curves as a function of metal orbital energy.

We have analyzed how the d electron count and d orbital energy affect the relative stability of the two competing structures of carbene complexes. For both structures **25** and **26** (models for these are **36** and **37**, respectively), a central metal occasionally takes up another axial ligand trans to the carbene moiety. Then how does an addition of an axial ligand influence the stability of the alternative structures? Although it is not easy to answer the question directly, we can say something about the trans effect on the stability of the M=C(carbene) bond in **25**. Considering the strong  $\sigma$ -donor and  $\pi$ -acceptor character of carbene fragment, we expect that an addition of a  $\sigma$  donor or a  $\pi$  acceptor would weaken the M=C bond, thus destabilizing **25**.

**Oxo-Iron Porphyrins.** Although isolation of the title molecules has not yet been achieved, they have been postulated to exist as important intermediates in enzymatic oxidation reactions.<sup>31a</sup> An oxo-iron intermediate is indicated by the stereochemistry of hydroxylation and epoxidation catalyzed by Cl-Fe-TPP or chlorodimethylferriprotoporphyrin.<sup>31b</sup> Recently the reaction of  $(Fe\text{-porphyrin})_2O_2$  with nitrogenous bases B was found to yield ferryl complexes  $(O=Fe\text{-porphyrin})(B)$ , which were characterized by spectroscopic and

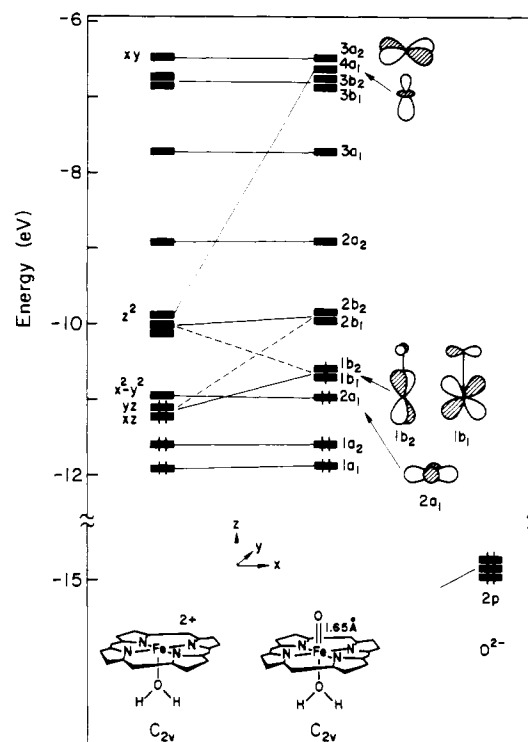
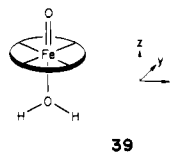


**Figure 7.** Interaction diagram for  $Fe(porphyrin)(OH_2)_2^{2+}$  and  $O^{2-}$  fragments of the oxo complex  $Fe(porphyrin)(OH_2)(O)$ .

chemical means.<sup>32</sup> The new complexes appear moderately stable at  $-80$  to  $-30$  °C. Then evidence has emerged from a mechanistic study that  $O=Fe\text{-porphyrin}$  is the active oxidant in iron(II) porphyrin catalyzed oxygenations of triphenylphosphine.<sup>33</sup>

Let us consider the bonding and electronic properties of ferryl complexes<sup>34</sup> using as a model compound  $(O=Fe\text{-porphyrin})(H_2O)$ . The structure of any ferryl complex is unknown. We assume a local pseudooctahedral geometry around the central iron atom, **39**. The iron atom is located



**39**

in the porphyrin plane,  $Fe=O$  set at  $1.65$  Å, while other geometrical parameters are the same as those in  $Fe(porphyrin)(CH_3)(H_2O)$  in Figure 5. The interaction diagram for  $Fe(porphyrin)(H_2O)_2^{2+}$  and  $O^{2-}$  is shown in Figure 7. The frontier orbitals of  $Fe(porphyrin)(H_2O)$ , on the left side of the figure, have been given in Figure 5. Three Fe d orbitals  $xz$ ,  $yz$ , and  $x^2 - y^2$  are low in energy, and  $xy$  is high above these three. The  $z^2$  orbital is also at low energy but is destabilized slightly by interaction with the axial  $H_2O$ . Further  $\sigma$  interaction with  $O^{2-}$  pushes the  $z^2$  orbital up high in energy ( $4a_1$ ), while the two  $\pi$  interactions destabilize  $xz$  ( $1b_1$ ) and  $yz$  ( $1b_2$ ). The two  $d_{\pi}$  orbitals split due to the noncylindrical  $H_2O$  but are almost degenerate. The  $\delta$ -type d orbital  $x^2 - y^2$  ( $2a_1$ ) remains untouched and stays at low energy. A nearly degenerate orbital set,  $xz$  ( $1b_1$ ) and  $yz$  ( $1b_2$ ), is available for the last two electrons of the complex, indicating a triplet ground state. Note that four electrons reside in M-O  $\pi$ -bonding levels,

(31) (a) For reviews on peroxidases see Dunford, H. B.; Stillman, J. S. *Coord. Chem. Rev.* **1976**, *19*, 187-251 and references therein. (b) Groves, J. T.; McClusky, R. E.; White, R. E.; Coon, M. J. *Biochem. Biophys. Res. Commun.* **1978**, *81*, 154-160 and references therein. (c) Groves, J. T.; Nemo, T. E.; Meyers, R. S. *J. Am. Chem. Soc.* **1979**, *101*, 1032-1033. (d) Groves, J. T.; Haushalter, R. C.; Nakamura, M.; Nemo, T. E.; Evans, B. J. *Ibid.* **1981**, *103*, 2884-2886.

(32) Chin, D.-H.; Balch, A. L.; LaMar, G. N. *J. Am. Chem. Soc.* **1980**, *102*, 1446-1448. Chin, D.-H.; LaMar, G. N.; Balch, A. L. *Ibid.* **1980**, *102*, 4344-4349.

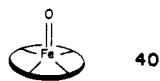
(33) Chin, D.-H.; LaMar, G. N.; Balch, A. L. *J. Am. Chem. Soc.* **1980**, *102*, 5945-5947.

(34) The  $Fe=O$  bond in ferryl complexes was discussed by: Ochiai, E. *Inorg. Nucl. Chem. Lett.* **1974**, *10*, 453-457.

two in  $\pi^*$ , so that an Fe=O double-bond notation is appropriate.

We have employed H<sub>2</sub>O as an axial ligand in order to compare the electronic structure of oxo-iron porphyrin with that of carbene-iron porphyrin (Figure 5) later in this section. The axial position in the biologically important oxoporphyrins is likely to be occupied by a base such as imidazole. However the difference in electronic properties between H<sub>2</sub>O and nitrogenous bases is not significant, in the sense that both act as weak  $\sigma$  donors in an axial coordination site of porphyrin complexes.

Another possible structure of oxo-iron porphyrins is a square pyramid which has no additional axial ligand, as shown in 40.



Removal of an axial  $\sigma$  donor from a pseudooctahedral geometry should stabilize the  $z^2$  ( $4a_1$ ) orbital. This trend was confirmed by a calculation on O=Fe-porphyrin: the Fe moved out of the porphyrin plane by 0.5 Å. The basic pattern of the interaction diagram of Figure 7 is carried over to O=Fe-porphyrin, except that the  $z^2$  ( $3a_1$ ) level is now at -9.4 eV instead of being at -6.6 eV.

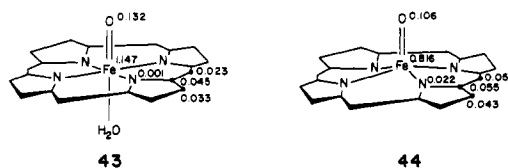
It is easy to understand why ferryl complexes are so unstable. Two electrons are in the  $xz$  ( $1b_1$ ) and  $yz$  ( $1b_2$ ) levels. These are antibonding combinations of Fe  $d_{xy}$  and O  $p_{xy}$  orbitals. Thus the Fe-O  $\pi$  bond is substantially weakened. If two or more electrons are removed from the ferryl system, one can get more stable oxometalporphyrin complexes. Examples of  $d^n$  ( $n < 4$ ) molecules are many: (O=M-OEP)(X) (M = Nb, X = F,  $d^0$ ; M = Mo, X = OMe,  $d^1$ ; M = W, X = OPh,  $d^1$ ; M = Re, X = OPh,  $d^2$ ), (O=M-OEP)<sub>2</sub>O (M = Nb,  $d^0-d^0$ ; M = Mo and W,  $d^1-d^1$ ; M = Re,  $d^2-d^2$ ),<sup>35</sup> O=V-porphyrin ( $d^1$ ) (porphyrin = etioporphyrin,<sup>37</sup> mesoporphyrin IX dimethyl ester, deuteroporphyrin IX dimethyl ester,<sup>38</sup> and TPP<sup>39,40</sup> O=M-tetramethyltetraethylcorrolate (M = Cr and Mo,  $d^1$ ), O=Re-octaethylcorrolate ( $d^2$ ),<sup>41</sup> O=Ti-tetra-*m*-tolylporphyrin ( $d^0$ ),<sup>42</sup> (O=Cr-TPP)(Cl) ( $d^1$ ),<sup>43</sup> and (O=Mo-TPP)(Cl) ( $d^1$ ).<sup>44</sup> Among these, X-ray diffraction analyses are available for (O=Mo-TPP)<sub>2</sub>O,<sup>36</sup> O=V-deoxyphylloerythroetioporphyrin, and (O=Mo-TPP)Cl.  $d^0$  Oxometalporphyrins sometimes have an extra ligand which sits cis to the oxygen atom, on the same side of the porphyrin plane, e.g., MoO<sub>2</sub>(TPP)<sup>44b</sup> (41) and (O=Nb-TPP)(OOC-CH<sub>3</sub>)(CH<sub>3</sub>COOH)<sup>45</sup> (42).



Recently Loew and Herman calculated by an INDO me-

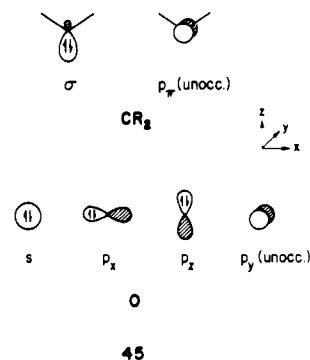
- (35) Buchler, J. W.; Rohbock, K. *Inorg. Nucl. Chem. Lett.* **1972**, *8*, 1073-1076.  
 (36) Johnson, J. F.; Scheidt, W. R. *Inorg. Chem.* **1978**, *17*, 1280-1287.  
 (37) O'Reilly, D. E. *J. Chem. Phys.* **1958**, *29*, 1188-1189. Pettersen, R. C.; Alexander, L. E. *J. Am. Chem. Soc.* **1968**, *90*, 3873-3875.  
 (38) Roberts, E. M.; Koski, W. S. *J. Am. Chem. Soc.* **1961**, *34*, 591-593.  
 (39) Kivelson, D.; Lee, S. *J. Am. Chem. Soc.* **1964**, *43*, 1896-1903. Assour, J. M. *Ibid.* **1965**, *43*, 2477-2489.  
 (40) A theoretical analysis of vanadyl porphyrin complexes is available in: Zerner, M.; Gouterman, M. *Inorg. Chem.* **1966**, *5*, 1699-1706.  
 (41) Murakami, Y.; Matsuda, Y.; Yamada, S. *Chem. Lett.* **1977**, 689-692. Matsuda, Y.; Yamada, S.; Murakami, Y. *Inorg. Chim. Acta* **1980**, *44*, L309-L311.  
 (42) Boreham, C. J.; Latour, J.-M.; Marchon, J.-C.; Boisselier-Cocolis, B.; Guillard, R. *Inorg. Chim. Acta* **1980**, *45*, L69-L71.  
 (43) Groves, J. T.; Kruper, Jr., W. J. *J. Am. Chem. Soc.* **1979**, *101*, 7613-7615.  
 (44) (a) Ledon, H.; Mentzen, B. *Inorg. Chim. Acta* **1978**, *31*, L393-L394. (b) Ledon, H.; Bonnet, M. *J. Chem. Soc., Chem. Commun.* **1979**, 702-704. Mentzen, B. F.; Bonnet, M. C.; Ledon, H. *J. Inorg. Chem.* **1980**, *19*, 2061-2066.

thod the spin density distribution in porphyrin-ferryl complexes which are models for intermediates in the enzymatic reactions of horseradish peroxidase HRP I and HRP II.<sup>46</sup> Our ferryl model of structure 39 is very close to the HRP II model ( $S = 1$ ). The calculated unpaired electron densities for 39 (in an open-shell configuration appropriate to  $S = 1$ ) are illustrated in 43. Most of the unpaired electrons reside on the



central Fe atom and some of them are distributed to the oxo ligand. Electron densities on atoms in the porphyrin ring are very small. These trends obtained here by extended Hückel calculations accord with the results of INDO calculations for the HRP II model.<sup>46</sup> The unpaired electron density distribution in the molecule 40 (again in an  $(xz)^1(yz)^1$  configuration) is given in 44. The out-of-plane displacement of the Fe=O group and the removal of an axial ligand increase the spin densities on the porphyrin ring, but only slightly.

It is interesting to compare the electronic structures of oxoiron porphyrins and those of carbeneiron porphyrins. If we think of an oxygen atom as neutral and put six valence electrons in 2s and two 2p orbitals, leaving 2p<sub>y</sub> vacant, 45, then



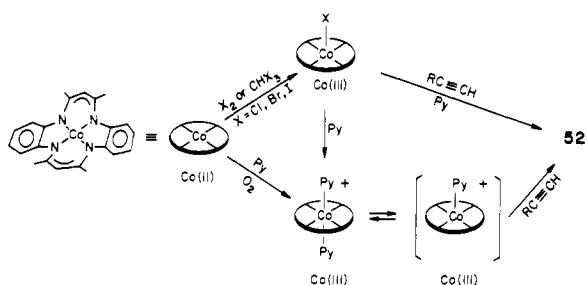
that configuration of oxygen and that of carbene are isoelectronic. Indeed, the carbene-oxygen analogy has figured prominently in discussions of biological oxygenation systems.<sup>47</sup> The similarities of O and CH<sub>2</sub> in their bonding to an iron porphyrin are apparent from Figures 5 and 7.

One major difference between O and CH<sub>2</sub> is that O has two  $p_x$  orbitals which interact with Fe  $d_{xy}$  orbitals while CH<sub>2</sub> has only one. The last two electrons of  $d^4$  (O=Fe-porphyrin)(H<sub>2</sub>O) enter the Fe  $d_{xy}$ -O  $p_x$   $\pi^*$  levels. In contrast the Fe  $d_{xy}$ -C  $p_x$   $\pi^*$  orbital of  $d^6$  (Fe-porphyrin)(CH<sub>2</sub>)(H<sub>2</sub>O) is unoccupied. Thus it is a carbene complex with two more electrons in the  $\pi^*$  orbital, i.e., a  $d^8$  carbene-nickel porphyrin of the structure 25 or 36, which is analogous to  $d^4$  (O=Fe-porphyrin). Both molecules should be, and are, relatively unstable.

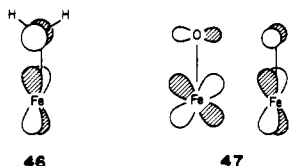
The other difference between O and CH<sub>2</sub> is their p ( $\pi$ ) orbital energies. The O p energy is much lower than the Fe d energy, while CH<sub>2</sub> p lies very close to Fe d. Thus the  $d_{xy}$ - $p_x$   $\pi$  (and  $\pi^*$ ) orbitals of O=Fe are more polarized than those of H<sub>2</sub>C=Fe. The  $\pi^*$  orbitals of H<sub>2</sub>C=Fe and O=Fe in

- (45) Lecomte, C.; Protas, J. *J. Chem. Soc., Chem. Commun.* **1976**, 434-435.  
 (46) Loew, G. H.; Herman, Z. S. *J. Am. Chem. Soc.* **1980**, *102*, 6173-6174.  
 (47) Hamilton, G. A. *Adv. Enzymol. Relat. Areas Mol. Biol.* **1969**, *32*, 55-96. In "Molecular Mechanisms of Oxygen Activation"; Hayaishi, O., Ed.; Academic Press: New York, 1974; pp 405-451.

Scheme I



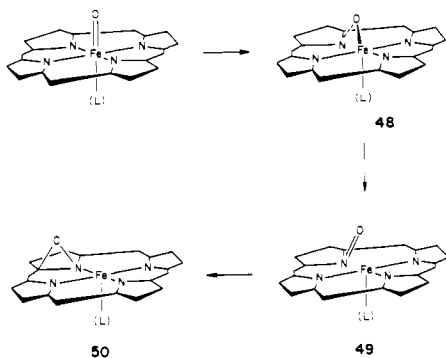
porphyrin complexes are compared schematically in **46** and **47**. As may be inferred from these drawings, the  $\pi^*$  anti-



bonding is diminished on going from  $X = \text{CH}_2$  to  $X = \text{O}$ . Population of the  $\pi^*$  by two electrons weakens both  $\text{Fe}=\text{CH}_2$  and  $\text{Fe}=\text{O}$  bonds but to a lesser degree for the oxygen complex. The replacement of Fe in **46** by Ni does not spoil the above line of argument. Therefore the instability of  $d^4$  ( $\text{O}=\text{Fe}$ -porphyrin)(L) should be less than that of  $d^8$  ( $\text{Ni}$ -porphyrin)(CRR') in geometry **25**, though both carry two  $d_{\pi} - p_{\pi} \pi^*$  electrons.

We intend to probe the oxenoid-carbenoid analogy in the future by actually calculating potential energy surfaces for the interaction of an (iron-porphyrin)=X ( $X = \text{O}, \text{CH}_2$ ) molecule with double bonds and CH groups.

Since  $d^4$  oxoiron porphyrins are formed by O-O bond cleavage of  $(\text{Fe}$ -porphyrin) $_2\text{O}_2$  or  $(\text{B}$ -Fe-porphyrin) $_2\text{O}_2$ , it seems natural to presume that their structure is **39** or **40**. Oxoiron porphyrins are very unstable and highly reactive species, though they have been detected spectroscopically at low temperatures.<sup>32</sup> The oxygen atom is readily transferred to organic and inorganic molecules. This intermolecular channel is one way for the labile oxygen atom to move. We wish to point out here that there is another possible channel, i.e., an intramolecular oxygen migration, as shown in **48**–**50**.

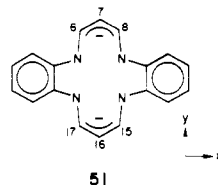


In light of the  $d^4$  ( $\text{O}=\text{Fe}$ -porphyrin)- $d^8$  ( $\text{Ni}$ -porphyrin)-(CRR') analogy, **48** might not be an unreasonable structure. More unprecedented would be the further O migration forming the structures **49** and **50**.

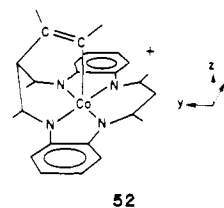
**Acetylene Addition to Co(TMTAA).** Dibenzo[*b,i*]-1,4,8,11-tetraazacyclotetradecinato dianion (TAA)<sup>48</sup> is one of a multitude of tetraazamacrocyclic ligands which, like porphyrins, contain a  $\text{N}_4$  donor core in a square-planar arrangement. Two major differences exist between TAA and porphyrins. One is the significantly short nitrogen to center

(48) The abbreviation TAA might be applied to any tetraazaannulene molecule. However, in this paper "TAA" is used specifically for dibenzotetraaza[14]annulenes, and likewise "TMTAA" stands for 6,8,15,17-tetramethyldibenzotetraaza[14]annulene.

(N-Ct) distance (1.85–1.87 Å) in TAA molecules.<sup>49</sup> The porphyrin N-Ct distance is about 2.01 Å. The other difference lies in the number of  $\pi$  electrons. A TAA dianion ligand carries 24  $\pi$  electrons, in contrast to the 26-electron porphyrin dianion. The negative charge of TAA dianions is considered to be delocalized over the 2,4-pentadiiminato chelates as shown in **51**.



The chemistry of dibenzotetraaza macrocycles has provided many intriguing compounds, many of which stem from the efforts of the Goedken and Dabrowiak groups.<sup>50</sup> Among the more interesting molecules to be prepared is the Co(III) complex of a novel pentadentate macrocycle with a vinylic carbon  $\sigma$  donor occupying one axial site, **52**.<sup>51</sup> Two reaction



sequences to **52** are shown in Scheme I.<sup>51a</sup> Both pathways are initiated by oxidation of Co(TMTAA) (TMTAA = 6,8,15,17-tetramethyl substituted TAA). Then cycloaddition of acetylene seems to take place across the six-membered chelate ring of the five-coordinated molecule Co(TMTAA)(py). The previous section on carbene complexes described several reactions in which a ligand traveled from the metal to the porphyrin ring. The case at hand is not quite a porphyrin. Nevertheless it shares with the previous reactions a coupling of metal and macrocycle chemistry, and as such caught our attention.

So that our theoretical analysis of the reaction can be simplified, TMTAA and the axial pyridine of the molecule **52** are replaced by TAA and  $\text{NH}_2^-$ , respectively. Thus we consider here an interaction between a model  $\text{Co}^{\text{III}}(\text{TAA})(\text{NH}_2^-)$  and acetylene.

At first we endeavor to understand the frontier orbitals of  $\text{Co}^{\text{III}}(\text{TAA})(\text{NH}_2^-)$ . In Figure 8 these are constructed step by step; from left to right, the planar TAA<sup>2-</sup> is deformed so as to reproduce the geometry of the TMTAA skeleton, then Co is incorporated in the middle of the TAA ring, and finally the fifth ligand  $\text{NH}_2^-$  is added from the bottom of the  $\text{CoTAA}^+$

(49) Weiss, M. C.; Bursten, B.; Peng, S.-M.; Goedken, V. L. *J. Am. Chem. Soc.* **1976**, *98*, 8021–8031.

(50) (a) Syntheses of dibenzotetraazaannulene were reported in: Hiller, H.; Dimroth, P.; Pfitzer, H. *Justus Liebig's Ann. Chem.* **1968**, *717*, 137–147. Jäeger, E. G. *Z. Anorg. Allg. Chem.* **1969**, *364*, 177–191. Chave, P.; Honeybourne, C. L. *J. Chem. Soc., Chem. Commun.* **1969**, 279. (b) Goedken, V. L.; Molin-Case, J.; Whang, Y.-A. *Ibid.* **1973**, 337–338. Goedken, V. L.; Park, Y.-A. *Ibid.* **1975**, 214–215. Weiss, M. C.; Goedken, V. L. *Ibid.* **1976**, 531–532. Goedken, V. L.; Peng, S.-M.; Park, Y.-A. *J. Am. Chem. Soc.* **1974**, *96*, 284–285. Goedken, V. L.; Pluth, J. J.; Peng, S.-M.; Bursten, B. *Ibid.* **1976**, *98*, 8014–8021. Goedken, V. L.; Park, Y.-A. *Ibid.* **1976**, *98*, 8391–8400. Gordon, G. C.; De Haven, P. W.; Weiss, M. C.; Goedken, V. L. *Ibid.* **1978**, *100*, 1003–1005. Weiss, M. C.; Gordon, G. C.; Goedken, V. L. *Inorg. Chem.* **1977**, *16*, 305–310. (c) Bell, L. G.; Dabrowiak, J. C. *J. Chem. Soc., Chem. Commun.* **1975**, 512–513. Neves, D. R.; Dabrowiak, J. C. *Inorg. Chem.* **1976**, *15*, 129–134. Woodruff, W. H.; Pastor, R. W.; Dabrowiak, J. C. *J. Am. Chem. Soc.* **1976**, *98*, 7999–8006. Nafie, L. A.; Pastor, R. W.; Dabrowiak, J. C.; Woodruff, W. H. *Ibid.* **1976**, *98*, 8007–8014. Fisher, D. P.; Piermattic, V.; Dabrowiak, J. C. *Ibid.* **1977**, *99*, 2811–2813. (d) See ref 2b and references therein.

(51) (a) Weiss, M. C.; Goedken, V. L. *J. Am. Chem. Soc.* **1976**, *98*, 3389–3392. (b) Weiss, M. C.; Gordon, G. C.; Goedken, V. L. *Ibid.* **1979**, *101*, 857–864.

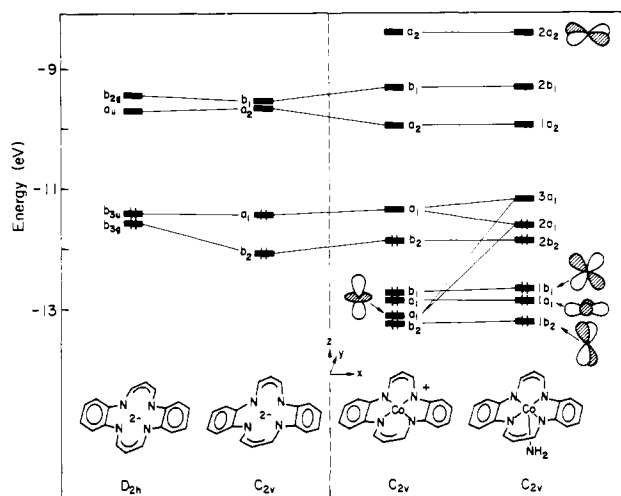
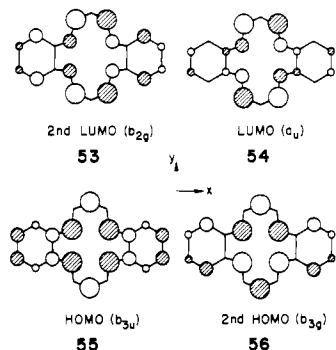


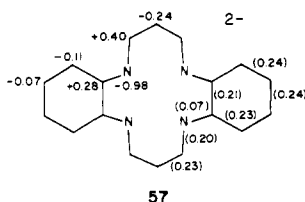
**Figure 8.** The building up of the orbitals of a  $\text{Co}(\text{TAA})(\text{NH}_2)$  fragment. From left to right: the orbitals of a planar  $\text{TAA}^{2-}$ ; the deformed  $\text{TAA}^{2-}$  in which two benzo groups are bent down by  $30^\circ$  while two allyl parts are bent up by  $25^\circ$ ; the  $\text{Co}(\text{III})$  complex of the deformed  $\text{TAA}^{2-}$ ; the orbitals of  $\text{Co}(\text{TAA})(\text{NH}_2)$ . Since the model ligand  $\text{NH}_2$  carries a  $-1$  electronic charge, the electronic configuration of  $\text{Co}$  in  $\text{Co}(\text{TAA})(\text{NH}_2)$  is  $d^6$ .

molecule. The planar  $\text{TAA}^{2-}$  carries 22  $\pi$  and  $\pi^*$  orbitals as well as combinations of four N lone pairs pointing toward the center of the ring. In Figure 9 we show only two HOMO's and two LUMO's which are characteristic of  $\text{TAA}^{2-}$ . These four orbitals are sketched in **53–56**. The circles indicate the



phase relationship of the top lobe of each  $\pi$  orbital. **55** and **56** will play a crucial role in the interaction with acetylene. The other orbitals are omitted from the figure.

Although the orbitals are delocalized over the entire  $\pi$  system, they may be recognized as primarily in-phase and out-of-phase combinations of  $\pi$  (or  $\pi^*$ ) orbitals of two 2,4-pentadiiminato chelates. The two LUMO's of TAA,  $b_{2g}$  and  $a_{1g}$ , contain the lowest unoccupied  $\pi$  orbital of the chelate anion, while the two HOMO's,  $b_{3u}$  and  $b_{3g}$ , contain the highest occupied  $\pi$  of the anion. The population analyses of  $\text{TAA}^{2-}$ , **57**, provide some further information. In **57** the numbers in parentheses are  $\pi$  overlap populations and those with signs indicate charges on atoms. The negative charge is distributed mainly over the four nitrogen atoms, as in a porphyrin ring. Significant deposits of negative charge are also seen at the  $\text{C}_7$  and  $\text{C}_{16}$  atoms. Another point in **57** is the small  $\pi$  overlap population between a nitrogen atom and a neighboring carbon

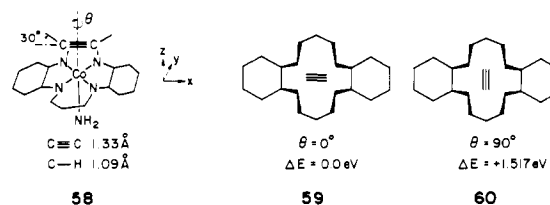


atom of benzene rings. The calculations thus support the importance of resonance structure **51** as a description of the molecule.

The structure of TMTAA is usually nonplanar. This is generally attributed to the steric interactions of the methyl groups in the 2,4-pentadiiminato linkages with the benzenoid rings. In complex **52**, the two pentadiiminato chelates warp up ( $\alpha$ ) and the two benzenoid rings bend down ( $\beta$ ) so that TMTAA in the complex has a pronounced saddle shape. In our calculations on the "deformed" TAA, the bending angles are assumed to be  $\alpha = 25^\circ$  and  $\beta = 30^\circ$ . Although the deformation reorganizes the molecular orbitals, the rough shapes of the  $b_{2g}$ ,  $a_{1g}$ ,  $b_{3u}$ , and  $b_{3g}$  orbitals (**53–56**) are retained in the  $b_1$ ,  $a_2$ ,  $a_1$ , and  $b_2$ , respectively, in the second column of Figure 9. Also the charge distributions and overlap populations are almost unchanged on going from the planar to the deformed TAA.

In the third column of Figure 8, the  $\text{Co}$  atom is incorporated. The molecule now carries five d orbitals in addition to the two HOMO's and the two LUMO's which correspond to the four orbitals of the planar or deformed TAA molecule. Because the d orbitals mix strongly with the TAA frontier orbitals, no pure d orbital can be assigned. The "five d orbitals" mean the five molecular orbitals with large d character. Of the four lowest lying of these, the " $z^2$ " is pushed up substantially by addition of the fifth ligand,  $\text{NH}_2^-$ , at the extreme right of Figure 8. The  $z^2$  orbital character is spread out over the LUMO ( $3a_1$ ) and the HOMO ( $2a_1$ ). We do not specify in the figure which orbital is classified as the d orbital, but the  $2a_1$  has a somewhat larger d orbital component than the  $3a_1$ . Note here that other TAA orbitals, the energy of which ranges from  $-12.0$  to  $-14.0$  eV, are omitted from the figure in order to avoid complexity. Actually these orbitals were found to be nearly free from interaction with acetylene in any conformation considered. It was also found that the two unoccupied levels  $2b_1$  and  $1a_2$  and the occupied  $1a_1$  are innocent of interaction. The important orbitals are the low-lying vacant  $3a_1$  and the occupied  $2a_1$ ,  $2b_2$ ,  $1b_1$ , and  $1b_2$ . Since the shapes of the  $3a_1$ ,  $2a_1$ , and  $2b_2$  are somewhat complicated, we show the contour diagrams of these three orbitals in Figure 9. This will help us analyze their interaction with acetylene. On the left side of the figure are the top views, contours in the plane parallel to the  $xy$  and  $1.0 \text{ \AA}$  away from the  $\text{CoN}_4$  unit in the  $z$  direction, while the right side gives the side views, contours in the  $yz$  plane. The structures of the other two orbitals,  $1b_1$  and  $1b_2$ , may be seen easily in the schematic orbital drawings of Figure 8.

The goal of this section is to understand why the reaction of  $d^6 \text{Co}^{\text{III}}(\text{TMTAA})(\text{py})^+$  with acetylene forms the 1,4-cycloadduct **52** and to find other possible stable (or metastable) adduct geometries if such exist. For this purpose, we have calculated two potential surfaces varying the conformation of an acetylene above  $\text{Co}(\text{TAA})(\text{NH}_2)$ . First we rotate the  $\eta^2$ -acetylene on the  $z$  axis, the center of the  $\text{C}\equiv\text{C}$  bond located  $1.91 \text{ \AA}$  above the  $\text{Co}$  atom (**58**). The two  $\text{C}-\text{H}$  bonds of the



acetylene are bent back, by  $30^\circ$  from linearity. The potential minimum is at  $\theta = 0^\circ$  (**59**). The energy increases monotonously with increasing  $\theta$  and reaches a maximum at  $\theta = 90^\circ$  (**60**).

Next the acetylene molecule is slipped off in the  $-x$  direction from **58** toward  $\eta^1$  coordination. A carbon atom of the

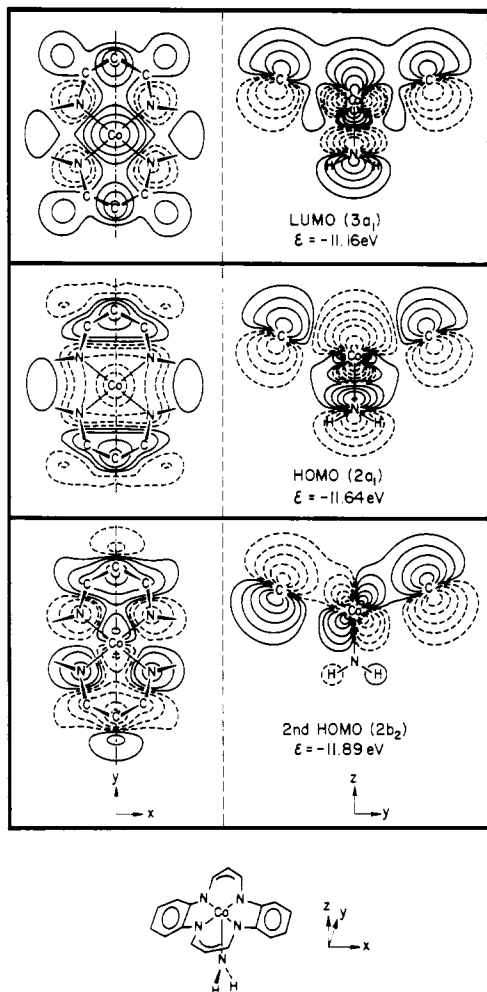
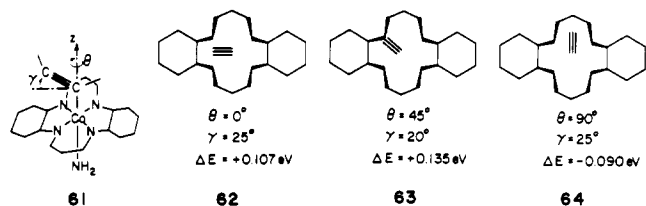


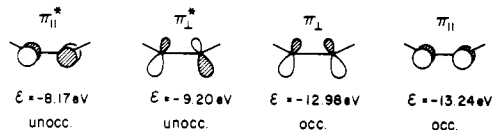
**Figure 9.** Contour plots of the three frontier orbitals of a  $\text{Co}^{\text{III}}\text{-(TAA)(NH}_2\text{)}$  fragment. The orbitals are shown in the  $xy$  plane (left) and in the  $yz$  plane (right). The contour levels of each diagram are  $\pm 0.003, 0.01, 0.025, 0.055, 0.1, 0.2,$  and  $0.4$ . The solid lines trace contours of one sign of  $\psi$ , the dashed lines of the opposite sign.

acetylene is placed  $1.91 \text{ \AA}$  above the Co atom. Then the  $\text{Co-C}\equiv\text{C}$  angle  $\delta$  and the swing angle  $\theta$  around the  $x$  axis are varied:  $\delta = 90\text{--}130^\circ$ ,  $\theta = 0\text{--}90^\circ$  (**61**). The energy minimum for a given  $\theta$  is at  $\delta = 25^\circ$  for  $\theta = 0^\circ$  (**62**),  $\delta = 20^\circ$  for  $\theta = 45^\circ$  (**63**), or  $\delta = 25^\circ$  for  $\theta = 90^\circ$  (**64**). A potential valley runs through these points. Total energies relative to that of **59** are given in **62–64** for each conformation. While



the potential curve along the valley seems rather flat, the overall energy minimum comes at  $\theta = 90^\circ$ , and  $\delta = 25^\circ$  (**64**).

On the two potential surfaces we have found two local minima. One is at the conformation **64**, which should lead to the 1,4-adduct **52**, while the other is at **59**. The conformer **64** was calculated to be  $-0.09 \text{ eV}$  more stable than **59**. To understand the potential energy surfaces let us consider the orbital interactions between  $\text{Co(TAA)(NH}_2\text{)}$  and acetylene. The frontier orbitals of  $\text{Co(TAA)(NH}_2\text{)}$  are already in our hands (Figures 8 and 9). A bent acetylene has four frontier orbitals which are derived from the two  $\pi$  and  $\pi^*$  sets, as shown in **65**.

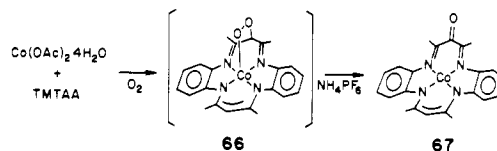


65

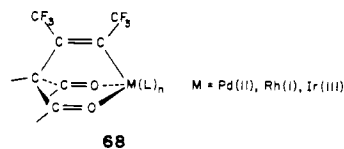
Let us superimpose the acetylene orbitals onto the frontier orbitals of  $\text{Co(TAA)(NH}_2\text{)}$  so as to see which orientation of the acetylene achieves effective orbital interaction. For the two equilibrium geometries **59** and **64**, the occupied  $\pi_{\perp}$  orbital of acetylene can overlap well with the  $3a_1$  LUMO of  $\text{Co(TAA)(NH}_2\text{)}$ . The unoccupied  $\pi_{\perp}^*$  is allowed to interact with the HOMO  $2a_1$  for **64** and with the low-lying  $1b_1$  for **59**. These interactions all stabilize the complex, and this must be why the two potential minima are at these two geometries. Conformers **62** and **63** do not find good bonding overlaps. Geometry **60** has possible interactions in the  $\pi_{\perp}-3a_1$  and  $\pi_{\perp}^*-1b_2$  pairs, as well as some in the  $\pi_{\perp}-2b_2$ . However, the aforementioned steric problem costs energy and makes this geometry unlikely. A minor repulsive interaction may be seen between the acetylene  $\pi_{\parallel}$  and  $1b_2$  (or  $1b_1$ ) for the  $\eta^2$  geometry **59** or **60**. For the slipped off geometries **62–64**, the repulsive interaction disappears or even becomes slightly attractive, due to a polarization of the  $\pi_{\parallel}$  and  $\pi_{\parallel}^*$  orbitals. We have described this type of polarization in discussing the  $\text{Fe=C=C}$  bond in the vinylidene carbene complex (**34**).

Just from the two potential surface cuts that we calculated, it is difficult to decide whether **59** or **64** should be more stable. In calculating the surfaces, we kept the saddle shape of TAA ( $\alpha = 25^\circ$ ,  $\beta = 30^\circ$ ) unchanged. Obviously this is not a good approximation if one intends to compare the absolute energies of the different adducts. Were one to move  $\text{C}_7$  upward in **64**, allowing stronger interaction between  $\text{C}_7$  and the terminal C atom of acetylene, the total energy would be much lowered. On the other hand, **59** can expect no further energy gain from any extra deformation of the TAA ring. Actually  $\text{Co(TMTAA)(py)(acetylene)}$  chooses the geometry **52**, with a chelate ring which is greatly deformed from geometry **64**. However, it may be that structure **59** exists as a stable or metastable molecule if the  $\pi_{\perp}^*-1b_1$  interaction is enhanced. This interaction should be increased if the metal has diffuse d orbitals with a high energy.

The reaction of a  $\text{Co}^{\text{III}}\text{(TMTAA)}$  complex with nitriles yielded 1,4-adducts very similar to the acetylene adduct **52**. Also the peroxo type intermediate **66** has been postulated in



the formation of the ring-oxidized molecule **67**.<sup>51a</sup> Thus 1,4-addition to  $\text{Co(TMTAA)}$  complexes seems to be a common course for unsaturated organic molecules. A somewhat related reaction may be the addition of the super dieneophile, hexafluorobutene, across the six-membered chelate ring of  $\text{Pd(II)}$ ,  $\text{Rh(I)}$ , and  $\text{Ir(III)}$  acetylacetonate complexes (**68**).<sup>52</sup>



68

**Acknowledgment.** Our work was generously supported by the National Science Foundation through Research Grant

(52) Barlex, D. M.; Evans, J. A.; Kemmitt, R. D. W.; Russell, D. R. *J. Chem. Soc., Chem. Commun.* **1971**, 331–332. Russel, D. A.; Tucker, P. A. *J. Chem. Soc., Dalton Trans.* **1975**, 1743–1748, 1749–1752.

Table I. Extended Hückel Parameters

orbital	$H_{ii}$	exponents <sup>a</sup>	
		$\xi_1$	$\xi_2$
Fe 4s	-8.39	1.90	
4p	-4.74	1.90	
3d	-11.46	5.35 (0.5366)	1.80 (0.6678)
Co 4s	-9.29	2.00	
4p	-5.35	2.00	
3d	-13.31	5.55 (0.5679)	2.10 (0.6059)
Ni 4s	-9.18	2.10	
4p	-5.15	2.10	
3d	-13.49	5.75 (0.5798)	2.3 (0.5782)
Rh 5s	-8.09	2.135	
5p	-4.57	2.100	
4d	-12.50	4.29 (0.5807)	1.97 (0.5685)
Re 6s	-9.22	2.398	
6p	-4.45	2.372	
5d	-11.29	5.343 (0.6359)	2.277 (0.5677)
H 1s	-13.60	1.30	
C 2s	-21.40	1.625	
2p	-11.40	1.625	
N 2s	-26.00	1.950	
2p	-13.40	1.950	
O 2s	-32.30	2.275	
2p	-14.80	2.275	

<sup>a</sup> Two Slater exponents are listed for the d functions. Each is followed in parentheses by the coefficient in the double- $\xi$  expression.

CHE 7828048. We are grateful to D. Mansuy and H. Ledon for communication of results prior to publication, to J. Jorgensen for the drawings, and to E. Stolz for the typing.

#### Appendix

All the calculations were of the extended Hückel type.<sup>53</sup>

The  $H_{ii}$ 's for Fe, Co, Ni, and Re were obtained from a charge iterative calculation on  $\text{Fe}(\text{NH}_2)_4^{2-}$  ( $d^6$ ),  $\text{Co}(\text{NH}_2)_4^-$  ( $d^6$ ),  $\text{Ni}(\text{NH}_2)_4^{2-}$  ( $d^8$ ), and  $\text{Re}(\text{CO})_5(\text{CH}_3)$  ( $d^6$ ). The  $(\text{NH}_2)_4$  unit is a planar model porphyrin (see the text). The A, B, and C parameters for the quadratic charge dependence of Re were assumed to be the same as those of Tc. Parameters used previously<sup>53</sup> for H, C, N, and O were kept fixed during the iteration procedures. The orbital exponents for Fe 3d, Co 3d, and Ni 3d are those given by Richardson et al.<sup>54</sup> while those for the 4s and 4p atomic orbitals are taken from previous work.<sup>55</sup> The Basch and Gray orbitals are used for the Rh and Re functions.<sup>56</sup> These extended Hückel parameters are listed in Table I.

**Note Added in Proof.** More examples of  $d^n$  ( $n < 4$ ) oxometalloporphyrins have appeared:  $\text{O}=\text{Mo}-\text{TPP}$  and  $\text{O}=\text{Mo}-(\text{tetra-}p\text{-tolylporphyrin})$ ,<sup>57a</sup>  $d^2$ ;  $\text{O}=\text{V}-\text{phthalocyanine}$ ,<sup>57b</sup>  $d^1$ ;  $\text{O}=\text{Mn}-\text{TPP}$ ,<sup>57c</sup>  $d^3$ ;  $(\text{O}=\text{Mo}-\text{TPP})(\text{OR})$  ( $\text{R} = \text{H}, \text{CH}_3, \text{Et}, i\text{-Pr}, t\text{-Bu}$ ),<sup>57d</sup>  $d^1$ .

Iron porphyrins with an oxene inserted into an iron-nitrogen bond (structure 48) have recently been proposed by two groups.<sup>58</sup>

- (53) Hoffmann, R. *J. Chem. Phys.* **1963**, *39*, 1397-1412.  
 (54) Richardson, J. W.; Nieuwpoort, W. C.; Powell, R. R.; Edgell, W. F. *J. Chem. Phys.* **1962**, *36*, 1057-1061.  
 (55) Summerville, R. H.; Hoffmann, R. *J. Am. Chem. Soc.* **1976**, *98*, 7240-7254. Albright, T. A.; Hofmann, P.; Hoffmann, R. *Ibid.* **1977**, *99*, 7546-7557.  
 (56) Basch, H.; Gray, H. B. *Theoret. Chim. Acta* **1966**, *4*, 367-376.  
 (57) (a) Diebold, T.; Chevrier, B.; Weiss, R. *Inorg. Chem.* **1979**, *18*, 1193-1200. (b) Ziolo, R. F.; Griffiths, C. H.; Troup, J. M. *J. Chem. Soc., Dalton Trans.* **1980**, 2300-2302. (c) Willner, I.; Otvos, J. W.; Calvin, M. *J. Chem. Soc., Chem. Commun.* **1980**, 964-965. (d) Ledon, H. J.; Bonnet, M. C.; Brigandat, Y.; Varescon, F. *Inorg. Chem.* **1980**, *19*, 3488-3491.  
 (58) (a) Chevrier, B.; Weiss, R.; Lange, M.; Chottard, J.-C.; Mansuy, D. *J. Am. Chem. Soc.* **1981**, *103*, 2899-2901. (b) Latos-Grazynski, L.; Cheng, R.-J.; LaMar, G. N.; Balch, A. L. *Ibid.* **1981**, *103*, 4270-4272.

Contribution from the Department of Chemistry, McMaster University, Hamilton, Ontario, Canada L8S 4M1

## Monomeric and Dimeric Thiodithiazyl Cations, $\text{S}_3\text{N}_2^+$ and $\text{S}_6\text{N}_4^{2+}$ . Preparation and Crystal Structures of $(\text{S}_3\text{N}_2)(\text{AsF}_6)$ , $(\text{S}_6\text{N}_4)(\text{S}_2\text{O}_2\text{F})_2$ , and $(\text{S}_6\text{N}_4)(\text{SO}_3\text{F})_2$

RONALD J. GILLESPIE,\* JAMES P. KENT, and JEFFERY F. SAWYER

Received July 30, 1980

The preparation and characterization by X-ray crystallography of two new examples of compounds containing the bis-(thiodithiazyl) cation,  $\text{S}_6\text{N}_4^{2+}$ , obtained from the reaction of  $\text{S}_4\text{N}_4$  with fluorosulfuric acid are reported. Crystals of the compound  $(\text{S}_6\text{N}_4)(\text{SO}_3\text{F})_2$  are monoclinic, of space group  $P2_1/c$  with  $a = 6.099$  (2) Å,  $b = 11.714$  (2) Å,  $c = 9.765$  (2) Å,  $\beta = 102.44$  (2)°,  $V = 681.3$  (3) Å<sup>3</sup>, and  $D_c = 2.18$  g cm<sup>-3</sup> for  $Z = 2$ . The structure was solved by direct methods and refined to final agreement indices  $R_1 = 0.029$  ( $R_2 = 0.039$ ) for 1239 observed reflections ( $I/\sigma(I) > 3.0$ ). Crystals of the compound  $(\text{S}_6\text{N}_4)(\text{S}_2\text{O}_2\text{F})_2$  are monoclinic, of space group  $C2/c$  with  $a = 12.108$  (4) Å,  $b = 10.350$  (3) Å,  $c = 12.045$  (3) Å,  $\beta = 104.82$  (3)°,  $V = 1459.2$  (8) Å<sup>3</sup>, and  $D_c = 2.18$  g cm<sup>-3</sup> for  $Z = 4$ . The structure was solved by direct methods and refined to final agreement indices  $R_1 = 0.036$  ( $R_2 = 0.041$ ) for 1089 observed reflections. It is noteworthy that, apart from the cation  $\text{S}_6\text{N}_4^{2+}$ , the latter compound also contains the previously unknown thiofluorosulfate anion, which shows rotational disorder about the sulfur-sulfur bond. It is shown that the cation in the compound reported to be  $(\text{S}_3\text{N}_2)(\text{AsF}_6)$  should also be formulated as a salt of the dimeric  $\text{S}_6\text{N}_4^{2+}$  ion, and an improved synthetic route to the compound  $(\text{S}_6\text{N}_4)(\text{AsF}_6)_2$  using the oxidation of  $\text{S}_4\text{N}_4$  with  $\text{S}_8(\text{AsF}_6)_2$  is also reported and discussed. Furthermore, it is shown by X-ray crystallography that the analogous oxidation of  $\text{S}_4\text{N}_4$  using the compound  $\text{Te}_6(\text{AsF}_6)_4$  gives, among other products, the first well-characterized example of a monomeric thiodithiazyl radical cation  $\text{S}_3\text{N}_2^+$ , again with hexafluoroarsenate as the counterion. Crystals of this compound are triclinic, of space group  $P\bar{1}$  with  $a = 9.471$  (4) Å,  $b = 5.645$  (2) Å,  $c = 7.843$  (3) Å,  $\alpha = 74.78$  (3)°,  $\beta = 90.53$  (3)°,  $\gamma = 97.99$  (3)°,  $V = 400.5$  (3) Å<sup>3</sup>, and  $D_c = 2.60$  g cm<sup>-3</sup> for  $Z = 2$ . The structure was solved by the heavy-atom method and refined to final agreement indices  $R_1 = 0.064$  ( $R_2 = 0.076$ ) for 1190 observed reflections. The significance of the strong cation-cation and anion-cation interactions in these salts of the monomeric and dimeric thiodithiazyl cations is discussed in terms of charge-transfer models.

#### Introduction

During the past few years the cyclic sulfur-nitrogen cations  $\text{S}_5\text{N}_5^+$ ,<sup>1-3</sup>  $\text{S}_4\text{N}_3^+$ ,<sup>4-9</sup> and  $\text{S}_4\text{N}_4^{2+}$ <sup>10</sup> have been prepared and

characterized by X-ray crystallography and other physical methods. There is however some confusion in the literature

(1) Roesky, H. W.; Bowing, W. G. *J. Chem. Soc., Chem. Commun.* **1975**, 735.

(2) Banister, A. J.; Durant, J. A.; Rayment, I.; Shearer, H. M. *J. Chem. Soc., Dalton Trans.* **1976**, 929.

(3) Hazell, A. C.; Hazell, R. G. *Acta Chem. Scand.* **1972**, *26*, 1987.